# Is higher resolution always better? A comparison of open-access DEMs for optimized Slope Unit delineation and regional landslide prediction

Mahnoor Ahmed[a], Giacomo Titti[b*], Sebastiano Trevisani[c], Lisa Borgatti[b], Mirko Francioni[a]

[a]Department of Pure and Applied Sciences, University of Urbino Carlo Bo, Urbino, 61029, Italy

[b]Department of Civil, Chemical, Environmental and Materials Engineering, ALMA MATER STUDIORUM University of Bologna, Bologna, 40126, Italy

[c]Dipartimento di Culture del Progetto, University Iuav of Venice, Venezia, 30135, Italy

[*]*Correspondence to*: Giacomo Titti (giacomo.titti@unibo.it)

**Abstract**

Digital Elevation Models (DEMs) play a key role in slope instability studies, ranging from landslide detection and recognition to landslide prediction. DEMs assist these investigations by reproducing landscape morphological features and deriving relevant predisposing factors, such as slope gradient, roughness, aspect, and curvature. Additionally, DEMs are useful for delineating map units with homogeneous morphological characteristics, such as Slope Units (SUs).

In many cases, the selection of a DEM depends on factors like accessibility and resolution, without considering its actual accuracy. In this study, we compared freely available global elevation models (ALOS, COP, FABDEM) and a national dataset (TINITALY) with a reference model (local airborne LiDAR) to identify the most suitable DEM for representing fine-scale morphology and delineating SUs in the Marche Region, Italy, for landslide susceptibility studies. Furthermore, we proposed a novel approach for selecting the optimal SUs partition.

The DEM comparison was based on several criteria, including elevation, residual DEMs, roughness indices, slope variations, and the ability to delineate SUs. TINITALY, resampled at a 30x30m pixel size, was found to be the most suitable DEM for representing fine-scale terrain morphology. It was then used to generate the optimal SUs partition among 18 combinations. These combinations were evaluated using both existing and newly integrated metrics alongside mapped landslide inventories to optimize terrain delineation and contribute to landslide susceptibility studies.

## 1. Introduction

Open-access global DEMs have been commonly used for a vast range of geomorphological studies, which have required modelling or analysis of terrain surface in mountain environments, where these DEMs have been characterized by a marked quality deterioration (Guth et al., 2024; Trevisani et al., 2023b). One of the many uses of DEMs has been to serve as the base input for analyzing landslides morphological features, state and style of activity and generating landslide susceptibility models (Brock et al., 2020). Among multiple methods of data-driven (Ahmed et al., 2023; Lombardo et al., 2020; Lombardo and Tanyas, 2020; Titti et al., 2021a) and physical-based models (Van den Bout et al., 2021) to predict, investigate (Brenning, 2005; Pirasteh and Li, 2017; Steger et al., 2023) and detect landslides (Qin et al., 2013), the elevation model has been of essential use. DEMs are utilized

to derive terrain-based characteristics (Brock et al., 2020; Mahalingam and Olsen, 2016) which have been conditioned by their resolution. In the literature, DEM resolution and its influence have been tested in several aspects such as: in landslide modelling and hazard assessment (Catani et al., 2013; Claessens et al., 2005; Fenton et al., 2013; Huang et al., 2023), in 3D physical models (Qiu et al., 2022), as well as morphological quality assessment explored at regional scales (Grohmann, 2018; Hawker et al., 2019; Trevisani et al., 2023b).

Comparisons among DEMs to evaluate the most suitable product are based on different criteria and the results have likely varied as per the test site. Thus, even if the same criteria have been used to rank DEMs, regional topography has influenced the preference of the elevation model in different areas (Florinsky et al., 2019; Zhang et al., 2019). Landcover has been specifically important when global DEMs (Bielski et al., 2024), such as Copernicus GLO-30 (COP) and Advanced Land Observing Satellite (ALOS) World 3D-30m, have been used for deriving a Digital Terrain Model (DTM), given that most of the times these products resembled more a Digital Surface Model (DSM: Guth & Geoffroy, 2021).

An ongoing initiative, the Digital Elevation Model Inter-comparison eXercise (DEMIX; Strobl et al., 2021), has aimed to align methodologies allowing for criteria-based ranking of global DEMs. In the first application (Bielski et al 2024), metrics related to slope and roughness have been considered in addition to those related to elevation differences; the approach has further developed, adopting new metrics and a wide range of geomorphometric derivatives (Guth et al., 2024). Global DEMs have been commonly used in geoscientific research due to their spatial extent and public accessibility whereas national DEMs (Gesch et al., 2018; Muralikrishnan et al., 2013; Tarquini et al., 2007) have generally been tailored to represent country-specific land surface and morphology at a higher spatial resolution and accuracy to serve geoscience applications. Shuttle Radar Topography Mission (SRTM; Jarvis et al., 2008), ALOS (Takaku et al., 2014), Terra Advanced Spaceborne Thermal Emission and Reflection Radiometer Global DEM (ASTER GDEM; Abrams et al., 2010) have been among the most widely used, freely accessible and initial global DEMs utilized in geomorphic analysis (Becek, 2014; Florinsky et al., 2019; Mahalingam and Olsen, 2016; Trevisani et al., 2023b; Zhang et al., 2019). However, several factors must be considered when implementing these global datasets in a localized area for landslide recognition, mapping, and assessment.

Landslide inventories and elevation models have been essential inputs for data-driven landslide models, for which the DEM has been used to derive morphological parameters such as slope angle and slope aspect. For these derivatives to be as accurate as possible in a model, the DEM quality (Claessens et al., 2005; Mahalingam and Olsen, 2016; Saleem et al., 2019) should satisfy the representation of fine-scale morphology (Chaplot et al., 2006; Florinsky, 1998). In other words, the DEM quality has significantly affected the prediction capacity of a model. The errors contained within a DEM, even when small, propagate in derivatives of elevation (Karakas et al., 2022; Mahalingam and Olsen, 2016; Pawluszek and Borkowski, 2017; Saleem et al., 2019) which have been weighed as important factors in landslide occurrence. The various available DEMs have been generated using a range of technologies. While significant efforts have been made to improve DEMs over time, the accuracy of these models has remained a critical issue. Selecting an appropriate DEM has proven to be more important than the number of DEM-derived factors used in landslide assessment (Kamiński, 2020).

Another use of DEMs has been the delineation of mapping units (Schlögel et al., 2018). Mapping units have been used to subdivide the study area in homogeneous, elemental units such as: administrative units (Lombardo et al., 2019), terrain units (Van Westen et al., 1997), unique condition units (Titti et al., 2021b), grid cells (Reichenbach

et al., 2018) or SUs (Ahmed et al., 2023). SUs were initially introduced by Carrara et al. (1991) as portions of territory, presenting homogeneous morphological characteristics for landslide identification and susceptibility mapping. The SU, according to the scale adopted, has served as a solution that adequately represents unstable slopes.

To assess the suitability of DEMs for landslide susceptibility and prediction, it has been essential to conduct a quality assessment of these models which has commonly referred to the spatial resolution alone. Therefore, global DSMs and a national Italian DTM has been compared with a local accurate elevation model (Airborne LiDAR) in the context of terrain representation and its delineation. The Italian DTM has been already investigated in some studies, mainly focusing on hydrogeomorphology studies (Pulighe and Fava, 2013; Zingaro et al., 2021; Annis et al., 2020; Tavares da Costa et al., 2019). Accordingly, the quality evaluation from the perspective of fine-scale morphology and geomorphometric derivatives in the context of landslide science has remained an interesting aspect to elaborate on.

This study has aimed to optimize inputs used for representing morphological data in landslide susceptibility assessment and to understand their interactions by: identifying the most suitable DEM for accurately representing fine-scale slope morphology; proposing a new metric for analyzing optimal SU parameters for landslide susceptibility mapping, integrating landslide inventory data with landslide area and numerosity; extending and applying the methodology to test landslide susceptibility at a regional scale in the Marche Region of Central Italy.

## 2. Study Area

In this study, we have selected two distinct study areas. The first Area of Interest (AOIa) has encompassed the entire Marche region, located in central-eastern Italy (Figure 1, AOIa). From the morphological point of view, this region is characterized by three different types of landforms that extend in the north-south direction. In the western part, the region has been crossed by the Apennines which can reach, in the area, a peak of 2476m a.s.l. at Monte Vettore. Then, the reliefs degrade to more rounded hills in the central part of the region till the flat eastern coastal strip. From a geological perspective, the Apennines, a Neogene fold-and-thrust belt that formed following the closure of the Mesozoic Tethys Ocean, is characterized by calcareous units, calcareous-marly and arenaceous units, as well as pelitic-arenaceous and marly-arenaceous units, ranging in age from the Jurassic to the Neogene. Several small rivers traverse the region from west to east. In particular, the basins of Misa, Esino, Cesano, and Metauro rivers were affected by an exceptional thunderstorm in September 2022, triggering floods and landslides (Corti et al., 2024). One of the highest rainfall intensity of the 2022 event was registered in a sub-portion of the Marche region, that has been selected as the second study area (AOIb) for this work (Figure 1, AOIb). This selection is not only based on the consequences of the exceptional rainfall event but also on the fact that, morphologically, it is typically representative of the mountainous terrain of Marche. Moreover, this area has been covered by a high-resolution dataset (1m pixel size) which allows us to effectively conduct the experiments as described in the following text.

A relevant portion of the territory of Marche region (AOIa) presents slope failures. The most populated dataset of landslide in the area is the inventory of the Piano stralcio per l'Assetto Idrogeologico (PAI) of Marche Region (Figure 1). In the area of Marche region (AOIa), the PAI counts 19,296 inventoried landslides for a total landslide

area of 1394 km$^2$ which covers 15% of the total regional surface classified as flow, slide and complex landslides (Cruden and Varnes, 1996).

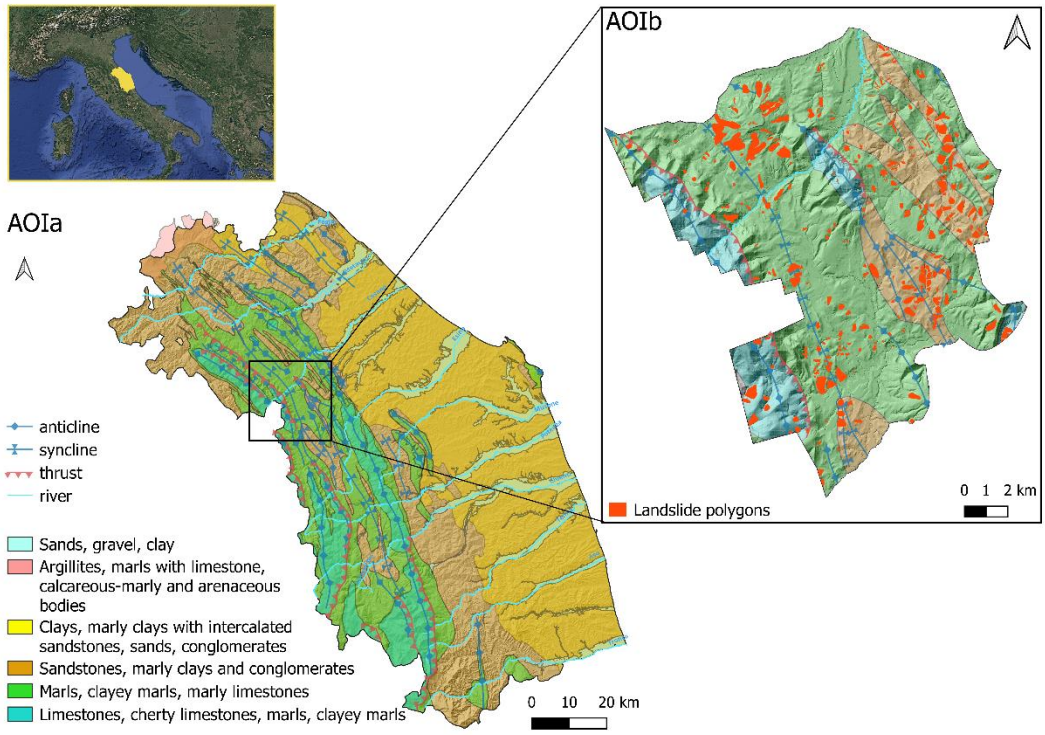


**Figure 1: Study area in central Italy. On the left, is the study area AOIa, encompassing the entire Marche region which has been analyzed in the second phase of the study. The geological classification is ordered by age (Quaternary, Cretaceous-Lower Pliocene, Lower Pliocene-Lower Pleistocene, Middle-Upper Miocene, Upper Eocene-Upper Miocene, Upper Trias-Middle Eocene) . On the right is study area AOIb, a sub-portion of the Marche region where we conducted the DEM analysis in the first phase covered by the 1m pixel size airborne LiDAR survey. The Piano Stralcio per l'Assetto Idrogeologico (PAI) landslide inventory of the Marche Region identifies 19,296 landslide bodies as polygons.**

## 3. Materials and Methods

The methodology implemented in this study has aimed to assess the quality of freely available DEMs, framing their use for landslide susceptibility assessment. DEMs have been essential because they allow the derivation of landslide predisposing factors and generate a morphology-based terrain subdivision: SUs. Thus, these two uses of a DEM in landslide susceptibility assessment have been investigated.

The analysis has been conducted in two sequential phases (Figure 2). In the first phase the differences in DEM derivatives have been assessed by comparing global and a national DEM to a local high-resolution reference elevation data in AOIb. In the second phase we have evaluated 18 SU partitions on the base of internal/external homogeneity, landslide extension and landslide number using the best performing open-source DEM, which has been identified in the first phase of this study.

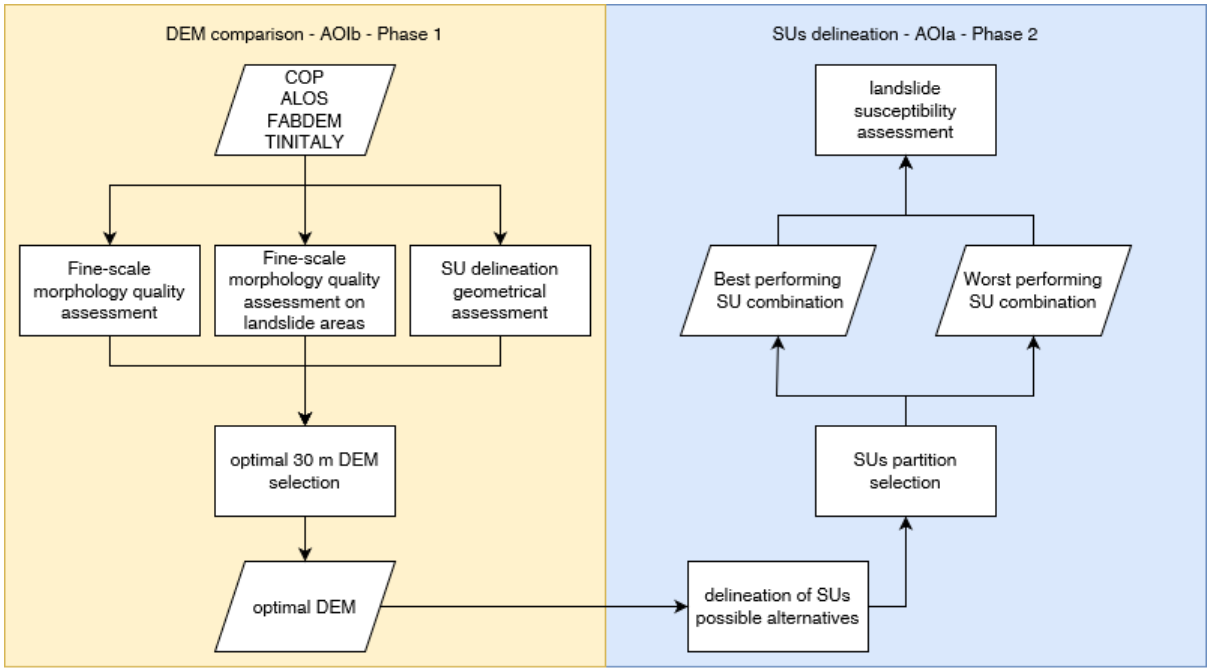


**Figure 2: Workflow of the two-phases analysis. Phase 1 DEM assessment: comparison of global and national DEM to a local high-resolution reference elevation model (with reference to AOIb). Phase 2 Slope Units delineation: selection of the optimal parameters for SUs delineation (with reference to AOIa).**

### 3.1. Phase 1: DEM assessment

In this phase, the accuracy of three global DEMs, as mentioned below, and one national DEM (TINITALY) has been evaluated by a comparison with a local airborne LiDAR in the study area AOIb.

ALOS (ALOS World 3D - 30m. V3.2, 2024) has been released by Japan Aerospace Exploration Agency (JAXA) in 2015, at a horizontal resolution of 1 arc-second, approximately 30 meters as a DSM (Caglar et al., 2018). This product, surveyed from 2006 to 2011, uses the 5-meter mesh of "World 3D Topographic Data" and is provided in two resampled versions by JAXA (mean resampling kernel is used in this study), with elevation expressed according to the Earth Gravitational Model 1996 (EGM96).

COP (European Space Agency, 2024), has been obtained from the WorldDEM at 1 arc second as a DSM, a product of the radar data acquisition of 12 meters TanDEM-X mission from 2011 to 2015. Forest And Buildings removed

COP DEM (FABDEM; Hawker et al., 2022), has been made available as a corrected global DTM available at 1 arc-second grid spacing (60°S-80°N) derived from COP. Machine learning techniques have been devised to improve mean absolute vertical error in built-up and forested areas in comparison to COP (Hawker et al., 2022). Both FABDEM and COP elevations have been referred to EGM 2008 geoid.

TINITALY's 1.0 (Tarquini et al., 2007), and version 1.1 (Tarquini et al., 2023), has covered the whole of Italian territory, as a DTM available at 10m pixel size. Heterogenous data, mainly based on Technical Regional Cartography (CTR) with elevations derived by means of photogrammetric method, has been used to build a national scale model. In particular, the CTR map scaled at 1:10000 with 10m interval for contour lines is used for Marche region in the compilation of TINITALY. A Triangular Irregular Network (TIN) structure has been employed in constructing the DEM to tackle varying data density and redundancy. Merging various types of input data is followed by significant investigation to ensure the seamless production of a high resolution and considerably the most accurate representation for Italy, with a root mean square error ranging from 0.1 to 6 meters (Tarquini et al., 2007).

The reference DEM (as called hereafter) has been a DTM acquired in 2012 using airborne LiDAR, with a pixel size of 1x1m, and a reported vertical and planimetric accuracy of 15 cm and 30 cm, respectively (Ministero dell'Ambiente e della Sicurezza Energetica, https://gn.mase.gov.it/portale/pst-dati-lidar). This reference DTM has been aggregated via averaging the pixel size to 30m.

The global DEMs (COP, FABDEM, ALOS) and TINITALY have been projected in WGS84 UTM 33N with a pixel size of 30 and 10 meters respectively using bilinear interpolation for alignment with the reference DEM. The inclusion of COP and FABDEM, along with ALOS as a global DEM and TINITALY as a national-scale elevation model for comparison, has been invoked by several studies (Bielski et al., 2024; Guth & Geoffroy, 2021; Meadows et al., 2024; Osama et al., 2023; Trevisani et al., 2023). All the DEMs, except TINITALY (geoid model not publicly available), have been transformed to a common geoid model, EGM2008 respectively for alignment and comparison with the reference grid. TINITALY is based on the Italian geodetic network (IGM95) where the measured ground points have been described by the Italian geoid called ITALGEO 2005 (Albertella et al., 2008; Barzaghi et al., 2007). Barzaghi and Carrion (2009) have concluded that the difference between ITALGEO05 (regional geoid model) and EGM2008 (global geoid model) is negligible for many applications, and both are capable to represent the region of Italy. Therefore, no geoid transformation for TINITALY has been required.

To perform the quality assessment of selected DEMs, elevation differences have been considered for compatibility with precedent studies. Indeed, studies focusing on DEMs comparison (Polidori and Hage, 2020) are generally based on elevation differences, using standard statistical metrics such as standard deviation and Root Mean Square Error (RMSE), and in some cases slope and aspect have been considered (Meadows et al., 2024; Zhang et al., 2019). However, as suggested in many studies (Bielski et al., 2024; Crema et al., 2020; Florinsky et al., 2019; Gesch, 2018; Guth & Geoffroy, 2021; Kakavas et al., 2020; Liu et al., 2019; Purinton & Bookhagen, 2017; Trevisani et al., 2023), statistical metrics of elevation differences alone fail to fully capture the quality of DEMs, including the capability to represent fine-scale morphology and the presence of artifacts. Therefore, for this reason and because the focus of the work has been to investigate mainly the accuracy of the DEMs geomorphometric derivatives, along with the differences in elevation, a straightforward and simple approach to take the local spatial variability of surfaces into account based on a geostatistical-based methodology (Isaaks and Srivastava, 1989), as discussed by Trevisani et al. (2023b), has been proposed.

The approach has been based on the derivation of a residual DEM, also known as Topographic Position Index (TPI; Guisan et al., 1999; Hiller and Smith, 2008; Wilson and Gallant, 2000), and the calculation of roughness indices. The residual DEM, derived by detrending the original surface, has permitted to highlight the capability of DEMs to reproduce local fine-scale morphology. Moreover, the residual DEM has been used as input for the calculation of roughness indices such as the standard deviation of residual DEM (Grohmann et al., 2011) or even geostatistical based estimators such as the variogram (Eq 1, with p = 2), the madogram (Eq. 1, with p = 1) and (Eq. 2) represents the more robust Median Absolute Differences (MAD; Trevisani and Cavalli, 2016; Trevisani and Rocca, 2015). The generalization of the variogram have been described as in Eq. (1) and MAD as Eq. (2);

$$\gamma(\boldsymbol{h})_p = \frac{1}{2N(\boldsymbol{h})}\sum_{\alpha=1}^{N(\boldsymbol{h})}|z(\boldsymbol{u}_a) - z(\boldsymbol{u}_a + \boldsymbol{h})|^p = \frac{1}{2}\cdot mean(|\Delta(\boldsymbol{h})|^p), \qquad (1)$$

where,

$$\Delta(\boldsymbol{h})_a = z(\boldsymbol{u}_a) - z(\boldsymbol{u}_a + \boldsymbol{h})$$

$$\mathrm{MAD}(\boldsymbol{h}) = |\Delta(\boldsymbol{h})_{\alpha=median}|, \quad (2)$$

where $\boldsymbol{h}$ is the separation vector (lag) between two locations $(u)$, $z(u)$ is the value of the variable of interest in the location $u$ (e.g., residual elevation), and $\mathrm{N}(\boldsymbol{h})$ is the number of point pairs with a separation vector $\boldsymbol{h}$ found in the search window considered. Accordingly, the variogram is the half of the mean squared differences $\Delta(h)_a$ and the MAD is the median of the absolute differences $\Delta(h)_a$. It should be highlighted that there are roughness indices such as $\mathrm{MAD}_{k2}$ and the Radial Roughness Index (RRI) that have been calculated directly from the DEM, without detrending (Trevisani et al., 2023c, a).

A simple short-range omnidirectional roughness index, such as MAD calculated for lag distances of 2 pixels and circular kernel of 3 pixels, permits to analyze fine-grain roughness (see Trevisani et al., 2023a; Trevisani and Rocca, 2015 for a full discussion). The MAD omnidirectional roughness index essentially provides a measure of omnidirectional spatial variability (median differences in residual elevation) by comparing all pixel values separated by a distance of |h| pixels in the moving window considered. An alternative roughness index which does not require the definition of calculation parameters is the RRI (Trevisani et al., 2023c), that has been derived to improve the popular Topographic Ruggedness Index (TRI; Riley et al., 1999).

All the comparisons have been done using a pixel size of 30x30m. This value was assumed because it is closer to the size of global 1 arc second DEMs, except for TINITALY which is released with a pixel size of 10x10m. TINITALY has been upscaled by mean-pixel aggregation to 30x30m pixel size. The 30m DEM (TINITALY30m) has also been compared with the 10m pixel size version (TINITALY10m) in AOIb to assess the effect of upscaling on the analysis. The aggregation at 30m permits to filter out or at least reduce some characteristics artifacts of TINITALY, such as triangular patterns, due to interpolation in areas of low data density, and artificial terraces, due to the interpolation of contour lines. Given that, slope, roughness indices and residual DEM are scale-dependent geomorphometric derivatives, a normalization has been done to compare the results of the differences between the derivatives at different resolutions of TINITALY and the reference DEM. Accordigly, a normalized difference has been adopted for each derivative D:

$$(D_{TINITALY} - D_{reference\ DEM}) \,/\, (D_{TINITALY} + D_{reference\ DEM}).$$

Finally, an additional analysis has been conducted. Since the goal of the research proposes attribution to landslide studies, the DEM-derived slope difference distribution in the landslide areas delineated by the PAI inventory is also included. To prevent overestimation of landslide areas, polygons contained within or significantly overlapping another polygon (primarily representing landslide reactivations) have been merged.

To further assist in evaluating the quality of DEMs in the frame of landslide susceptibility assessment, the SUs have been generated using various DEMs (global and national). This has allowed for a comparison of the SUs produced from the reference DEM with those derived from the global DEMs under evaluation, highlighting any differences in terrain partitioning and geometry. The software r.slopeunits (Alvioli et al., 2016) has been used to generate the SU maps, starting from the SU parameters proposed by Alvioli et al. (2016) for AOIb. After a few corrections and optimizations, the parameters have been set as: flow accumulation threshold to $5\times10^5$ $m^2$, minimum SU area as 80,000 $m^2$, circular variance as 0.4 and clean size of 60,000 $m^2$ with the cleaning method (flag -m) that removes SU smaller than the clean size as well as removes odd-shaped polygons and SUs with width as small as two grid cells (Alvioli et al., 2016). To quantify the similarity between SUs derived from reference DEM and from each DEM under observation, the Jaccard Index (Jaccard, 1901) has been utilized to estimate Intersection-over-Union (IoU) ratio between the reference (in this case SU derived from reference DEM) and the predicted (in this case the DEM under test). The Jaccard Index can measure the segmentation of the SU in reference to the overlapping of the defined shape and similarity of terrain-representation. Ranging from 0, signifying no similarity, to 1 that signifies identical sets, this index considers the combined size which is inclusive of the intersection. Hence, the higher the index value, the better delineation of terrain as per the considered reference.

### 3.2. Phase 2: Slope Units delineation

This phase of the work has been focused on the identification of the most representative and freely available DEM to subdivide the study area in SUs for landslide modelling. Therefore, 18 SUs partitions have been generated with r.slopeunits software and then compared with landslide areas and landslide counts mapped in the AOIa to find the optimal ones. The optimal DEM obtained from the first phase has been used to test SU delineation in the study area with a range of parameters. As proposed by Alvioli et al. (2016), an aspect segmentation metric has been used to analyze the optimal parameters for the Marche region, altering two parameters: the minimum surface area of SU and the minimum circular variance for terrain, and fixing the parameters flow accumulation and clean size.

The aspect segmentation metric has been based on the concept of partitioning terrain by grouping pixels sharing similar aspect properties. This has been transferred to SU delineation, with the assumption, given the partitioning has been evaluated by the internal homogeneity and external heterogeneity of SU. The aspect segmentation metric can be written as:

$$F(a,c) = \frac{V_{max} - V}{V_{max} - V_{min}} + \frac{I_{max} - I}{I_{max} - I_{min}} \quad , \quad (3)$$

where $V$ (SU homogeneity) is the local aspect variance and $I$ is the autocorrelation which represents the external heterogeneity of the adjacent SUs and $F$ evaluates the morphometric delineation of the SUs, explained by the minimum surface area of a SU ($a$) and the minimum circular variance ($c$) (see for more details, Alvioli et al., 2016). The first term of $F$ value is estimated based on the homogeneity of pixels grouped in a single SU, thus a higher value represents a better segmentation. In the same way, on the base of the second term of Eq. 3, the greater

the difference between the average aspect value of each SU and each of the relative adjacent SU, the higher is the $F$ value. Overall, from a geometrical point of view the optimal $a$ and $c$ combination is the one that maximizes the metric value.

Differently from Alvioli et al. (2016) where the Area Under the Curve (AUC) derived from landslide susceptibility assessment has been also considered in selecting the optimal SU parameters, this study proposes to compare the landslides extension ($A$) and landslide density ($D$) per SU. The former sums the percentage of the landslide area included inside the SU where the failure has been triggered (from the initiation point). The latter is the inverse of the average number of landslides in each SU. $A$ and $D$ can be expressed as;

$$A = \frac{\sum_{i=1}^{N} l_i}{L_i} \quad (4)$$

$$\frac{1}{D} = \frac{\sum_{i=1}^{N} d_i}{N} \quad (5)$$

where $L_i$ , in Eq. 4, is the total landslide area of all the events triggered in the $i^{th}$ SU, $l_i$ is the cumulative landslides area inside the $i^{th}$ SU which excludes the extension of landslide that occupies adjacent SUs, $N$, in Eq. 5, is the number of unstable SUs, $d_i$ is the number of landslides triggered in the $i^{th}$ SU.

$$S(a,c) = \frac{F(a,c)-F_{min}(a,c)}{F_{max}(a,c)-F_{min}(a,c)} \cdot \frac{A(a,c)-A_{min}(a,c)}{A_{max}(a,c)-A_{min}(a,c)} \cdot \frac{D(a,c)-D_{min}(a,c)}{D_{max}(a,c)-D_{min}(a,c)} \quad (6)$$

where $S$ is the final metric which combines $F$, $A$ and $D$. The optimal combination of $a$ and $c$ for SU delineation in the study area selected is the one that maximizes the $S$ metric in Eq. 6. SU parameters for the experiment on entire Marche region have been tested with; flow accumulation threshold to $10\times10^5$ m$^2$, clean size of 20,000 m$^2$ with the cleaning method (flag -m). Minimum area ($a$) has been tested with 40, 80, 150, 200, 300 and $500\text{x}10^3$ m$^2$ with corresponding circular variance ($c$) of 0.1, 0.4 and 0.7 for each $a$, making 18 combinations.

The Susceptibility Zoning plugin (SZ-plugin), integrated with QGIS and developed by Titti et al. (2022), has been used to calculate the aspect segmentation metric ($F$) and to map the landslide susceptibility in the Marche region (AOIa). This analysis has utilized the DEM selected in Phase 1 and assessed four SU delineations, ranked from highest to lowest performance, as mapping units for evaluating landslide susceptibility. The analysis has been conducted using a Generalized Additive Model (Loche et al., 2023). The covariates selection includes: lithology, from national dataset (http://portalesgi.isprambiente.it/), landcover (2018 CORINE, https://land.copernicus.eu/en) as categorical covariates. The continuous covariates have been generated using the Spatial Reduction Tool (Titti et al., 2022) from the phase 1-selected DEM as derivatives; slope angle, planar and profile curvature as ordinal covariates and northness, eastness as linear covariates. The collinearity between the predisposing factors has been evaluated by the Pearson's coefficient. The results have been validated with a 10-fold spatial cross-validation which clusters the dataset with a k-means approach (Elia et al., 2023). The overall prediction capacity has been estimated with ROC-based AUC (Fawcett, 2006), F1 score (Singhal, 2001) and Coen's Kappa score (K; Kraemer, 2015).

## 4. Results

The differences between elevation, residual DEMs, roughness indices and slope variations within the four selected open-access DEMs and the reference DEM have been shown in Figure 3. The boxplots report the distribution of the differences higlighting the median, the first and the third quartile excluding the outlayers. Moreover, since the differences report positive and negative values, the absolute mean difference has been calculated. Therefore, the lower the variance and the absolute mean difference, the better is the output considered.

Overall, TINITALY resampled at 30m (TINITALY30m) has showcased the best performance across all metrics, with a smaller distribution of differences and lower absolute mean difference. ALOS, on the other hand, has displayed the largest difference among all DEMs across all metrics. Between COP and FABDEM, COP has shown a larger distribution of elevation differences, and as expected, COP has had a stronger tendency to overestimate elevation with respect to FABDEM (Figure 3). However, for slope (Figure 3B) and isotropic roughness (Figure 3C), FABDEM has displayed more spread in differences.

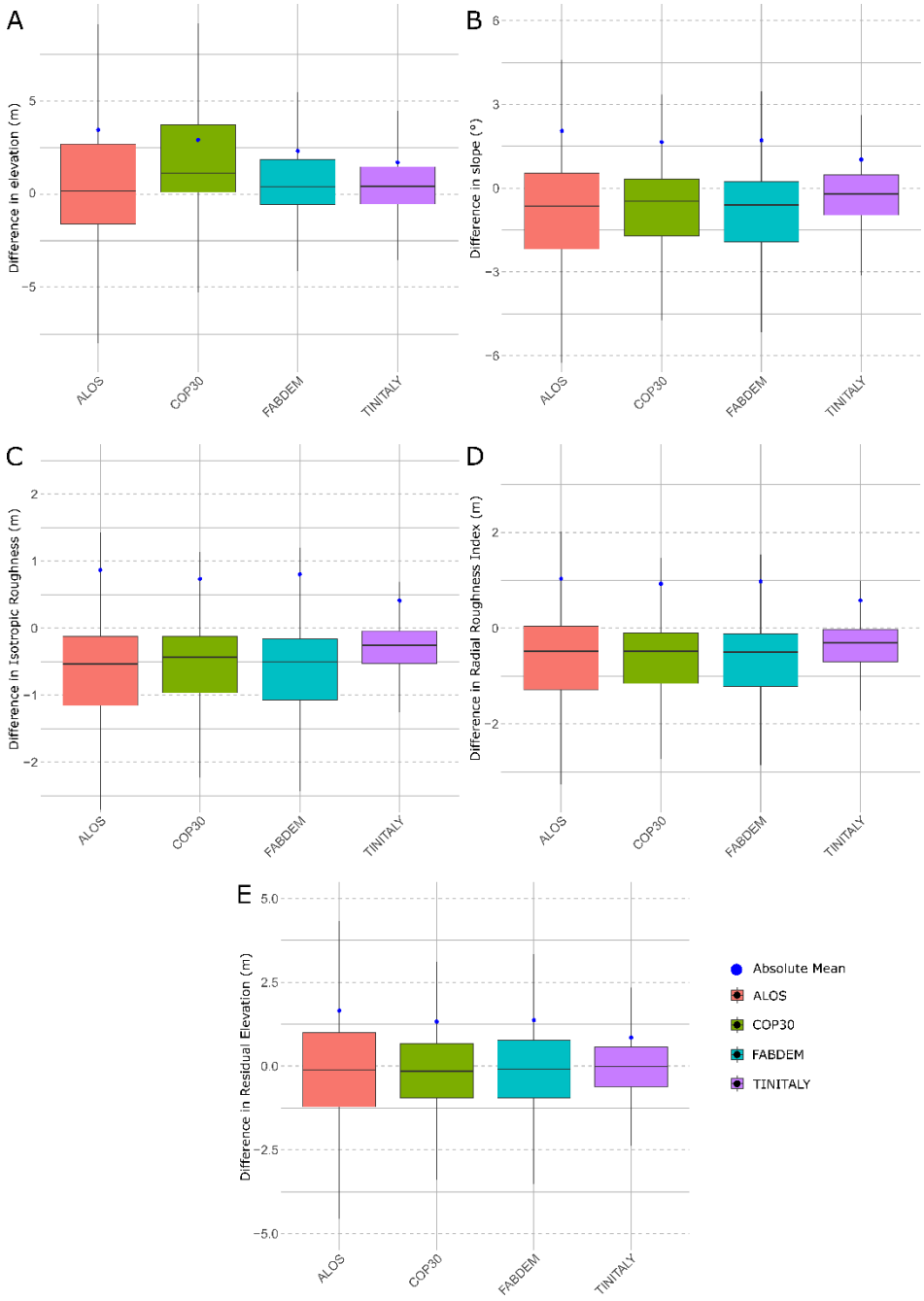


**Figure 3:Boxplots visualizing the differences among the DEMs at 30 meters, using different metrics with the absolute mean calculated; A) Elevation, B) Slope, C) Isotropic Roughness Index, D) Radial Roughness Index and E) Residual DEM.**

Figure 4 exhibits the differences of the selected derivatives between TINITALY30m and TINITALY10m. Apart the elevation, TINITALY at 10m is quantifying a larger distributions in normalized differences for the terrain indices. The absolute mean difference confirms the trend.

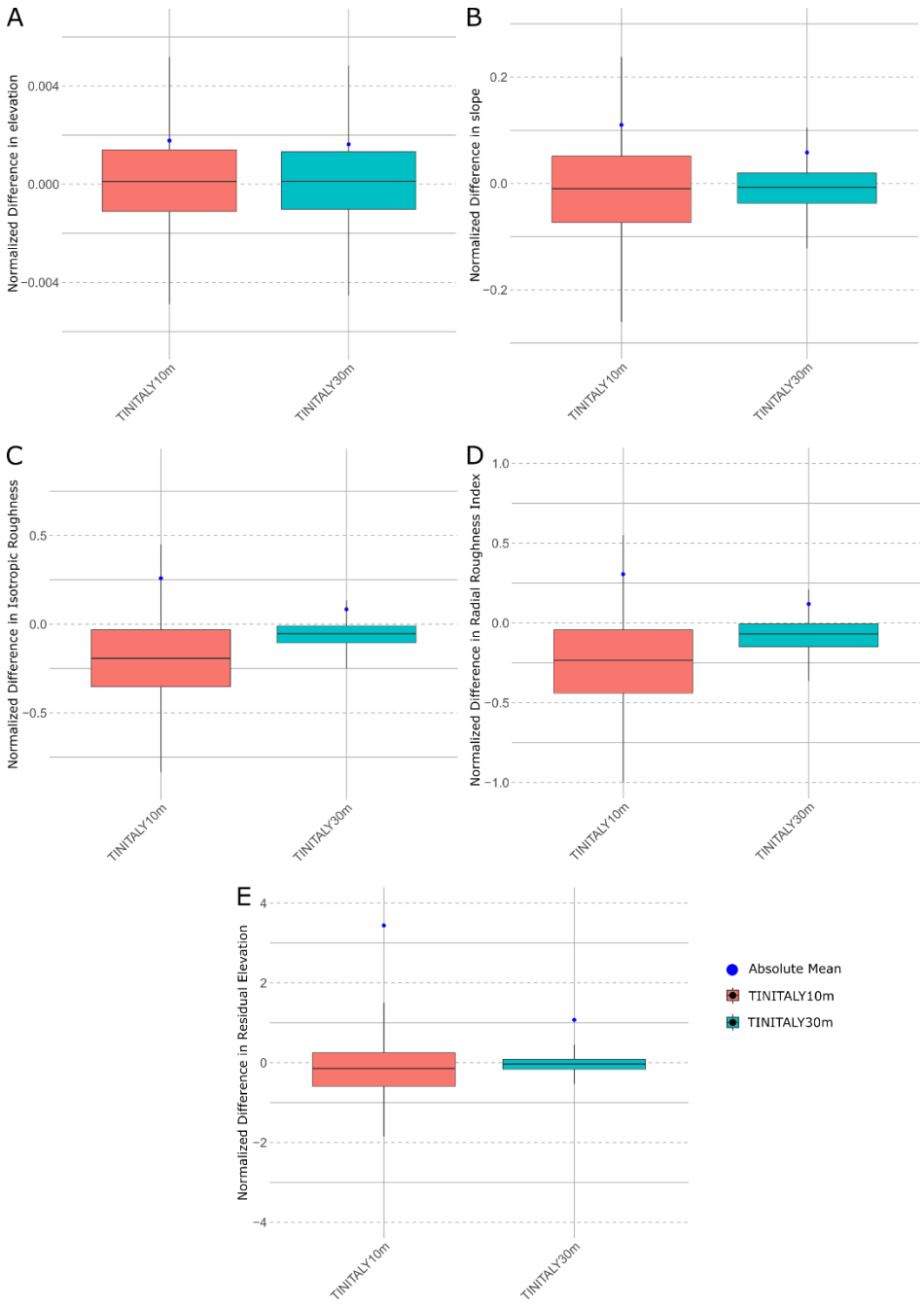


**Figure 4: Boxplots showing the differences in TINITALY at 10m and 30m with respect to the reference LiDAR at the respective resolution, for different indices with the absolute mean calculated; A) Elevation, B) Slope, C) Isotropic Roughness Index, D) Radial Roughness Index and E) Residual DEM.**

Since the main topic of our analysis is to support landslide susceptibility mapping, we have investigated the performance of the selected DEMs to derive slope, which is considered one of the most relevant landslide predisposing factors, in the area where landslide bodies have been mapped. Figure 5 shows the slope-difference within the mapped polygons of the PAI landslide inventory. TINITALY30m is seen to have the smallest differences in terms of absolute mean and the distribution among all the other DEMs (Figure 5A). Similarly, in Figure 5B, the distributions of the normalized differences of TINITALY 10m and 30m clearly highlight the larger differences distribution of the 10m DEM.

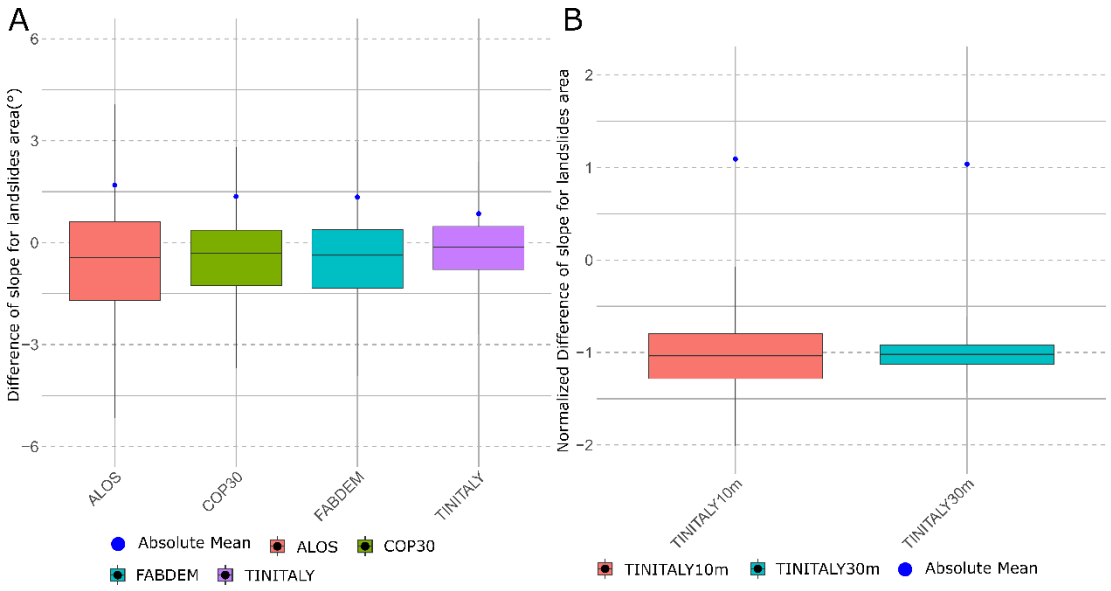


**Figure 5: A) Slope differences for 30m DEMs as compared to the reference DEM in PAI landslide polygons. B) Normalized difference in slope with reference DEM for 10m and 30m TINITALY in PAI landslide polygons.**

The last part of the DEMs comparison would investigate the effect on the SUs delineation of different DEMs. Table 1 reports the Jaccard index tested comparing the SUs delineated with DEMs at 30m and SU generated with the reference DEM. The highest similarity index is for TINITALY30m.

**Table 1: Jaccard Index represented as Intersection-over-union for SUs generated from the DEMs under test with the reference LiDAR DEM SUs.**

| **DEM** | **IoU** |
|---|---|
| ALOS | 0.866 |
| FABDEM | 0.896 |
| COP | 0.887 |
| TINITALY30m | 0.912 |

The second phase of the analysis has been focused on the optimal SUs delineation to assess landslide susceptibility in AOIa. Since in the previous analysis TINITALY30m has been found as the most accurate DEM to represent the morphology of the mountainous area of the Marche region, we have generated 18 SU combinations based on TINITALY30m to find the optimal SUs partition of AOIa. Figure 6 shows the visual differences in delineation for some of the parameter combinations. Smaller values of circular variance and minimum area result in smaller dimensions of SUs which can restrict heterogeneity between adjacent SUs while, ideally, SUs should maintain external heterogeneity for better terrain representation.

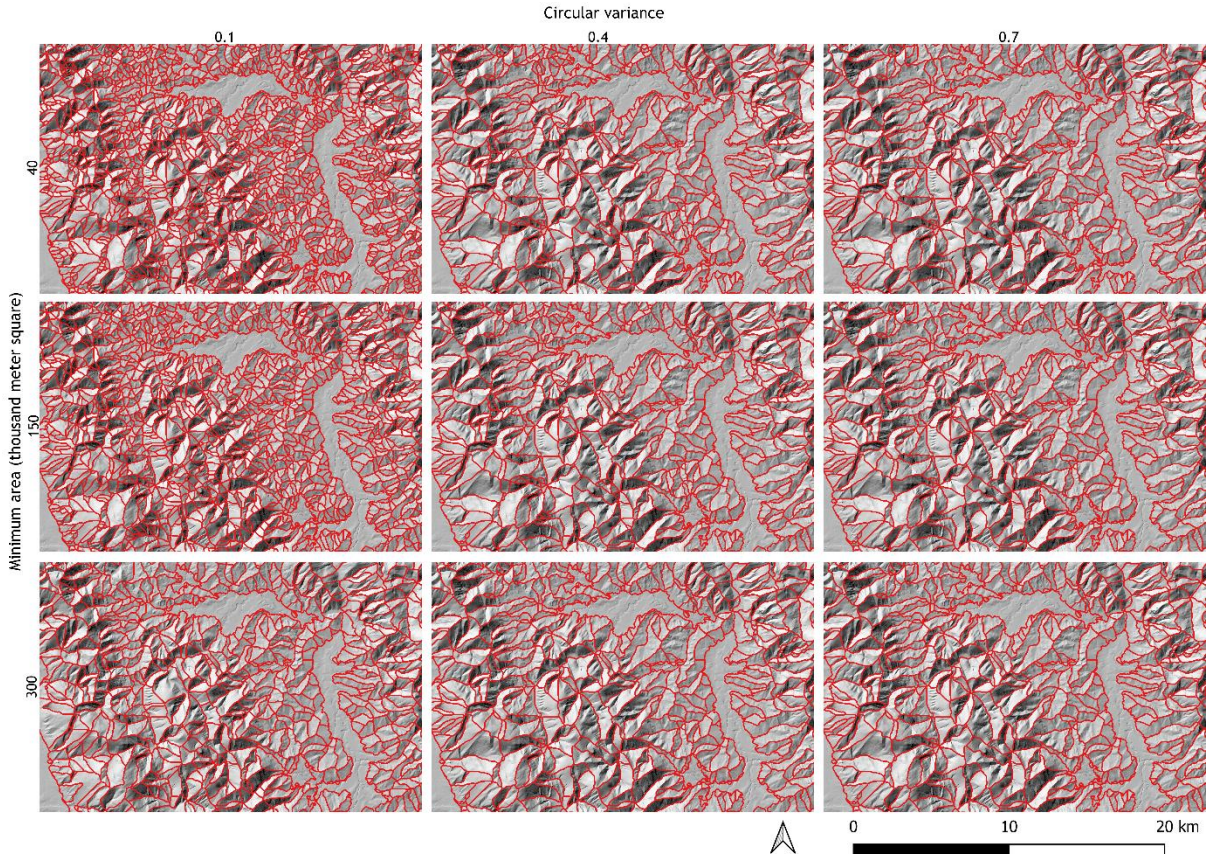


**Figure 6: SU combinations. 9 out of the 18 combinations are shown to highlight differences as the values of two parameters change, i.e., minimum area and circular variance.**

Figure 7 reports the behavior of the *F, A* and *D* metrics and the final S metric based on the 18 combinations of *a* and *c*. Considering that each of the metric represents a goodness for the final SU partition, higher the *F, A* and *D*, better is the SU partition. Excluding *F,* which shows an almost irregular pattern with the maximum at *c* equal to 0.1 and *a* equal to $40x10^3m^2$ (Figure 7.1). *A* and *D* have a mutually opposite almost linear pattern which reach a maximum pairing: in A where *c* is equal to 0.7 and *a* is each of the values assigned (Figure 7.2), in *D* with *c* equal to 0.1 and *a* equal to $40x10^3m^2$ (Figure 7.3). *A* shows a better performance increasing the mapping unit extension of the study area, whereas *D* shows better performance with smaller partitions.

The product of the normalized metrics results in the *S* value which is maximized in the range of *a* between $300x10^3$ $m^2$ and $200x10^3$ $m^2$ and by a value of 0.1 for *c* (Figure 7.4). Therefore, among the tested combinations, *c* equal to 0.1 and *a* equal to $300x10^3$ $m^2$ produce the optimal SU partition for landslide susceptibility mapping in the Marche region with a SU extension of 0.40 $km^2$ on average (dataset freely available on Ahmed and Titti, 2024). On the contrary the worst-case partition is the one which combines *c* equal to $150x10^3$ $m^2$ and *a* equal to 0.7 with a SU extension of 0.84 $km^2$ on average.

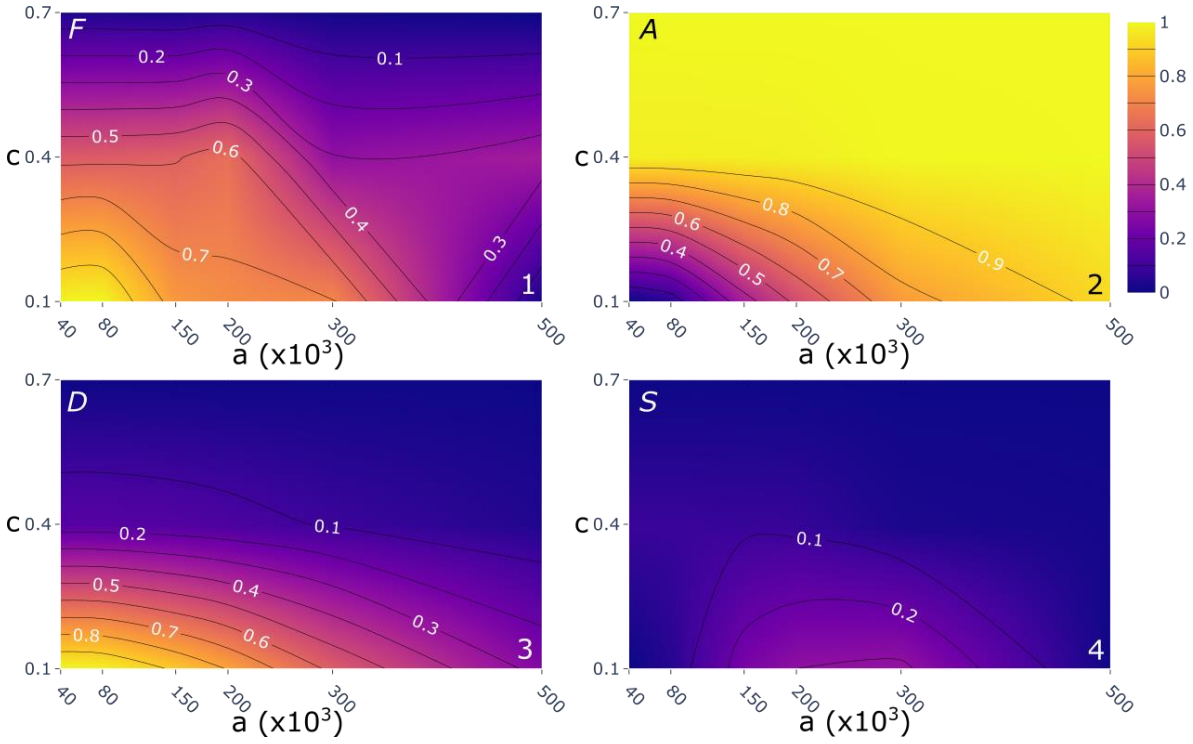


**Figure 7: Behavior of the *F, A* and *D* metrics and the final S metric with respect to parameters *a* and *c*: (1) shows the F value of SU aspect segmentation metric, (2) visualizes the landslide extension inside a SU (*A*), (3) shows the landslide density (*D*) and (4) depicts the results of the final combined metric *S*.**

Consequently, the susceptibility assessment with the S-optimal and S-worst case SUs partition has been carried out. The maps resulting from the susceptibility analysis and the relative confusion matrixes based on the S-optimal and the S-worst case SUs delineation of TINITALY30m dataset are represented in Figure 8, while the quality metrics generated from the 10-fold spatial cross validation by ROC analysis are reported in Figure 9. The summary of these metrics is provided in Table 2.

**Table 2: Summary of confusion matrix from maps in Figure 8 and performance metrics in Figure 9.**

| | True Positive (TP) | True Negative (TN) | False Positive (FP) | False Negative (FN) | AUC | F1 score | Cohen's Kappa Index |
|---|---|---|---|---|---|---|---|
| S-optimal | 37% | 6% | 31% | 26% | 0.68 | 0.6 | 0.23 |
| S-worst case | 45% | 6% | 24% | 25% | 0.74 | 0.67 | 0.29 |

In addition, two more landslide susceptibility analysis have been carried out using SUs partitions with intermediate S values: *c* equal to 200x10$^3$ m$^2$ and *a* equal to 0.4, *c* equal to 40x10$^3$ m$^2$ and *a* equal to 0.1, to investigate the relation between AUC and the number, or extension, of the slope units (see Sect. 5)

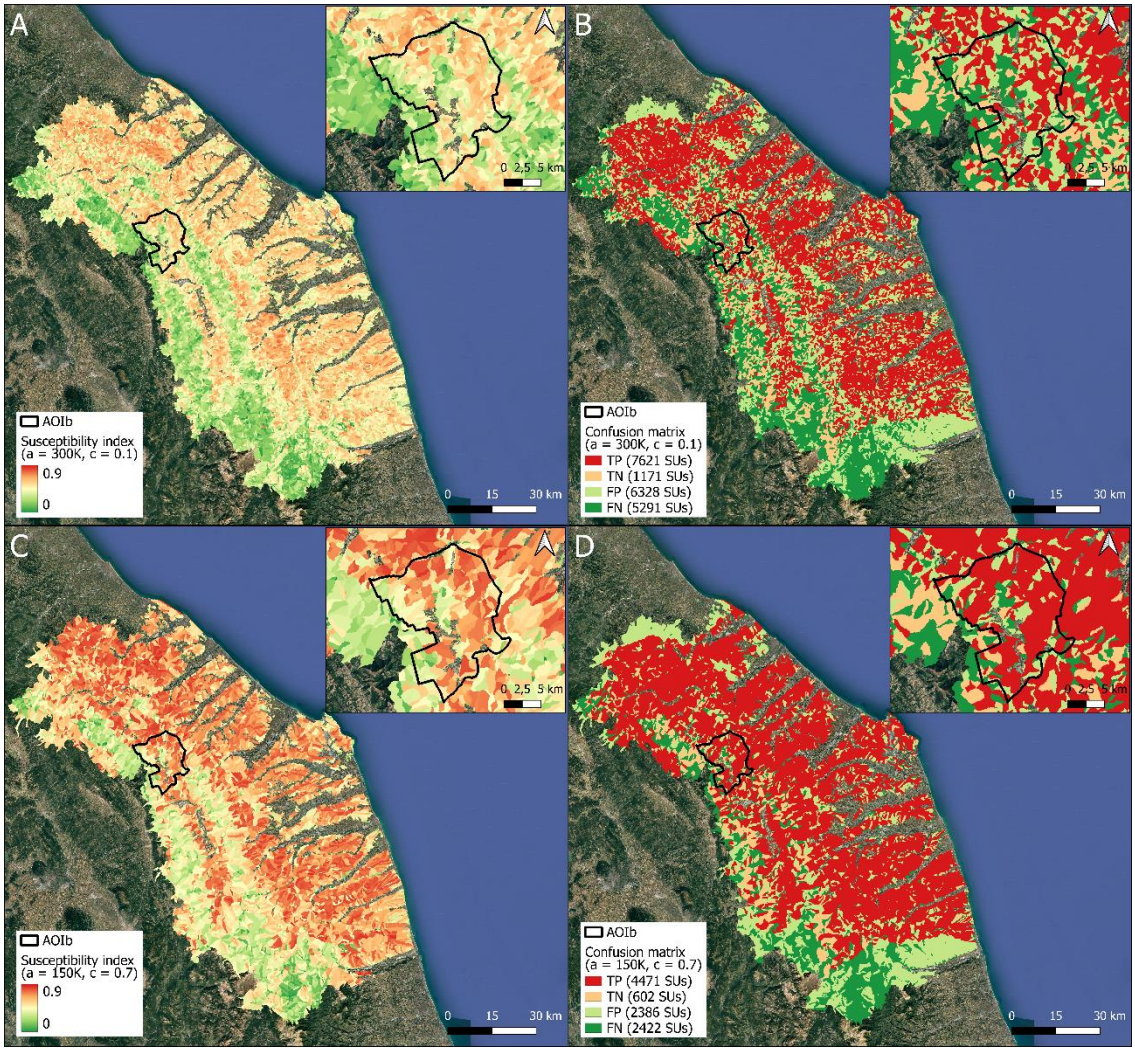


371

372 **Figure 8: Landslide susceptibility mapping with TINITALY 30m using: A) the selected optimal SU delineation**
373 **(a=300x10$^3$ m$^2$, c=0.1) with the relative confusion matrix (B) (TN 6% of all and 13% of unstable units); C) the selected**
374 **worst case SU delineation (a=150x10$^3$ m$^2$, c=0.7) with the relative confusion matrix (D) (TN 6% of all and 12% of**
375 **unstable units). Image background from © Google Maps 2019.**

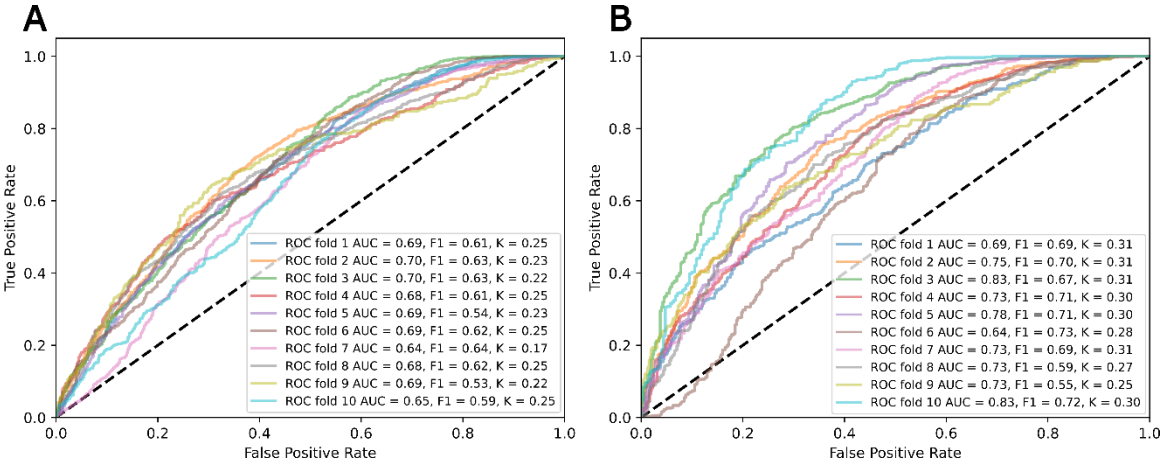


376

377 **Figure 9: ROC curve with AUC, F1 score and Kappa coefficient values for 10-fold cross validation. A) the optimal SUs**
378 **delineation (a=300x10$^3$ m$^2$, c=0.1); B) the worst-case SUs delineation (a=150x10$^3$ m$^2$, c=0.7).**

## 5. Discussion

Based on the results of the quantitative comparison between ALOS, COP, FABDEM, TINITALY10m and TINITALY30m, the latter has performed better than the other DEMs as per the indices used in this study (Figure 3). These comparisons are insightful for morphological differences for instance, in regard to roughness indices (Figure 3D), all DEMs tend to oversmooth with respect to the reference DEM. This can be indicative of the spatial support being larger than 30m in reality, meaning that the spatial data density is much lower than the given resolution. It is also interesting to realize the difference between COP and FABDEM. FABDEM (DTM) being a product of COP (DSM), in essence should be closer to the LiDAR representation of the terrain with vegetation and buildings removed, but it produces a less accurate output. The efforts of generating a DTM from COP have been motivated in the application of flood modelling trying to optimize the terrain representation, especially in areas of relatively low elevation. However, the algorithm has not been devised for optimizing geomorphometric derivatives such as slope (Hawker et al., 2022). This can be particularly relevant when modelling slope instability. Thus, FABDEM in the region considered does not improve the terrain representation as compared to COP (Bielski et al., 2024). This behavior is visible in Figure 3 where FABDEM shows larger difference distributions than COP for slope, residual DEM and both roughness indices. For instance, in regard to roughness indices (Figure 3D), all DEMs tend to oversmooth with respect to the reference DEM which can be indicative of the spatial support being larger than 30m in reality, meaning that the spatial data density is much lower than the given resolution.

ALOS consistently features high differences in all computed metrics against the counter global DEMs which could be explained with the analysis of Caglar et al. (2018). They concluded that ALOS contains a significant number of anomalies in elevation values, possibly attributed to unfiltered sensor noise and processing algorithms which are often not easily identifiable. Nonetheless, ALOS is still ranking well above other global products like SRTM and NASADEM according to quantitative assessments on DEM derived parameters and is still comparable with COP and FABDEM (Bielski et al., 2024; Guth et al., 2024).

The numerical comparisons resulting in Figure 3 can be supported by the graphical representation of the slope differences in Figure 10. Although the spatial distribution of differences varies, larger differences are most noticeable in the ALOS DEM, followed by COP and FABDEM, compared to TINITALY30m, which exhibits fewer differences in slope compared to the reference DEM.

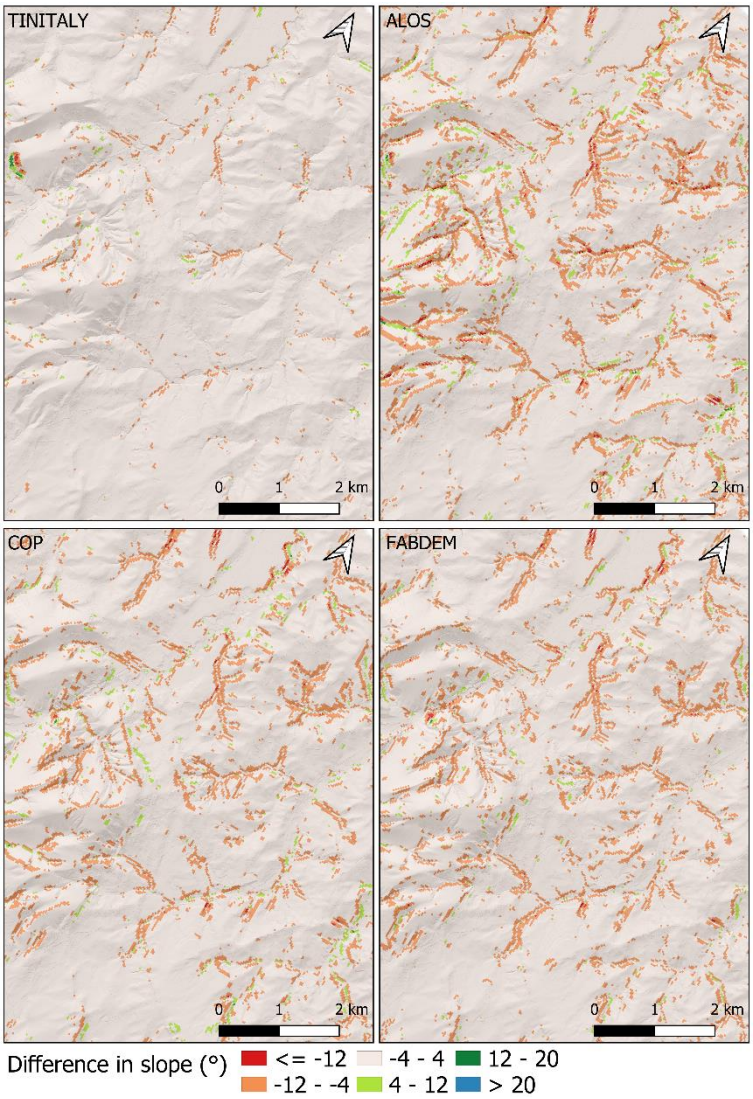


406

407 **Figure 10: Difference in slope (degrees) between the four tested DEMs (30m) and the reference LiDAR DEM, by**
408 **subtracting the LiDAR value from the test DEM value.**

409 TINITALY was originally published with a pixel size of 10x10m. Since the pixel sizes of the open global DEMs
410 selected to be compared with the reference DEM in the AOIb area are around 30x30m, we have decided to conduct
411 the entire analysis using the same grid-cell size of 30m. Therefore, the original TINITALY10m has been resampled
412 to 30x30m cell size. Despite this, the accuracy of TINITALY10m has been also investigated where we have
413 compared the performance of TINITALY30m and of TINITALY10m using normalized differences instead of
414 simple differences. Although this was not the primary aim of the study, the tests indicate that TINITALY at 30m
415 pixel size outperforms the 10m pixel size (Figure 4). These differences in performance, apart from the expected
416 lower uncertainty related to the larger spatial support, may be attributed to the interpolation approach used for
417 TINITALY10m. In areas with low sampling density, noticeable artifacts appear, which can significantly affect the
418 calculation of geomorphometric derivatives. Resampling from the original 10m pixel size to a coarser one (30m)
419 can partially filter out these artifacts. Thus, higher resolution does not necessarily guarantee better results if it is
420 not supported by high-quality elevation data or if it contains a high number of artifacts (Chen et al., 2020;
421 Mahalingam and Olsen, 2016). Additionally, the use of contour lines as input data for TINITALY 10m along with
422 triangulator for interpolation may result in spurious spikes at regular intervals within elevation zones and in areas

with triangular slope-faces (Zingaro et al., 2021). Considering the acquisition dates of DEMs in comparison to the LiDAR, COP and ALOS have been surveyed closer to the time of the LiDAR than TINITALY but even so, TINITALY30m has shown better results when compared with the LiDAR. Comparing slope differences in landslide areas across the selected global open-access DEMs, as well as TINITALY10m and TINITALY30m, yield similar results. The graphs in Figure 5 present similar distribution of relative differences in Figure 3 and Figure 4. Comparing slope differences in landslide areas across the selected global open-access DEMs, as well as TINITALY10m and TINITALY30m, yield similar results.

The similarity between the geometry of delineated SUs with the same parameters, as compared with the ones delineated from the reference DEM, indicates a higher value of the Jaccard Index for TINITALY30m. This means that the SUs delineated using TINITALY30m most closely resemble those from the reference LiDAR DEM. The remaining of the global DEMs also produce SUs with a high similarity index.

In the end of Phase 1, we can conclude that for the Marche region, the use 30m resampled TINITALY DEM is recommended for SU definition, therefore the rest of the analysis proposed for Phase 2 has been based on TINITALY30m.

Extending the analysis of SU delineation from AOIb, we have used multiple SU parameters for a more detailed analysis in AOIa with landslide polygons. Understandably, slope-facing direction and slope angle can be considered as driving factors for slope failures and can be used to dissect the terrain into units which can morphologically describe landslide prone areas. Landslide susceptibility evaluates the probability of occurrence of a landslide according to a set of variables. Susceptibility depends upon a set of variables whose values are associated in a unitary manner to each mapping unit. Therefore, the mapping unit represents a portion of territory that each variable describes numerically by a single value as if it was a point object. Consequently, the smaller the dimension of the mapping unit, the more representative the single variable is. However, a spatial event such as a landslide, which is a non-point event, does not represent a homogeneous object according to the variables chosen to predict it (i.e., the degree of slope is not homogeneous throughout the landslide area). Thus, to evaluate the probability of occurrence of this event, it is necessary to identify unique values for each chosen predictor calculated within a portion of territory that coincides as much as possible with the landslide. It is also comprehensible that including stable areas, the portion of territory that most closely resembles the landslide area is the slope-aspect which can be represented by the SU. Therefore, to satisfy both the needs described above, the mapping unit should be as concise as possible to describe the shape of the landslide area.

The methodology adopted to evaluate the SU subdivision has been designed to address the forementioned requirements by integrating new metrics, specifically tailored for landslide studies considering the relevance of terrain units with landslide inventories. In addition to the aspect segmentation metric ($F$) proposed by Alvioli et al. (2016), the landslide extension coefficient ($A$) and the landslide density coefficient ($D$) have also been included. In a way, the $F$ metric can define the shape of the SU on the base of the spatial aspect distribution (Figure 11A and Figure 11B), while a balance between $A$ and $D$ can define the extension of the SU.

According to $A$, the optimal SUs are the ones that contain the entire landslide, with no landslide area falling in adjacent SUs. The landslide coefficient $A$ may not fully capture the extent of landslide area especially when dealing with landslides characterized by high mobility, as in the case of flow-like landslide which can reach considerable distances where the run-out may move out from the homogenous slope-aspect. Nevertheless, the

462 frequency distribution of the landslide classes in the landslide inventory will balance the *A* value, therefore the
463 run-out of flow-like landslides may have an impact on the SU dimensions if their presence is significative in the
464 inventory. Otherwise, part of the unstable area may fall in the adjacent SUs. Consequently, the larger the SU is,
465 the higher is the probability of including the entire landslide, as is visible in Figure 11C and Figure 11D where an
466 example of the lowest and highest performing SU partition according to *A* is represented. In contrast to *A*, the *D*
467 metric would avoid the overestimation of the SU dimension which should be limited, ideally, to a single landslide
468 (see the example in Figure 11E and Figure 11F). A correct use of *D* metric requires that reactivated landslides
469 should be excluded and considered as unique events, to avoid doubling the number of polygons in the same spatial
470 unit.

471 The variability of the SU extension with respect to the parameters *a* and *c* can also be described through the
472 number of unstable units in relation to the total number of SUs. Figure 12 shows how as *D* increases and *A*
473 decreases, the unstable units increase. At the same time as *D* increases and *A* decreases, the SU extension is
474 reduced and therefore SU count increases.

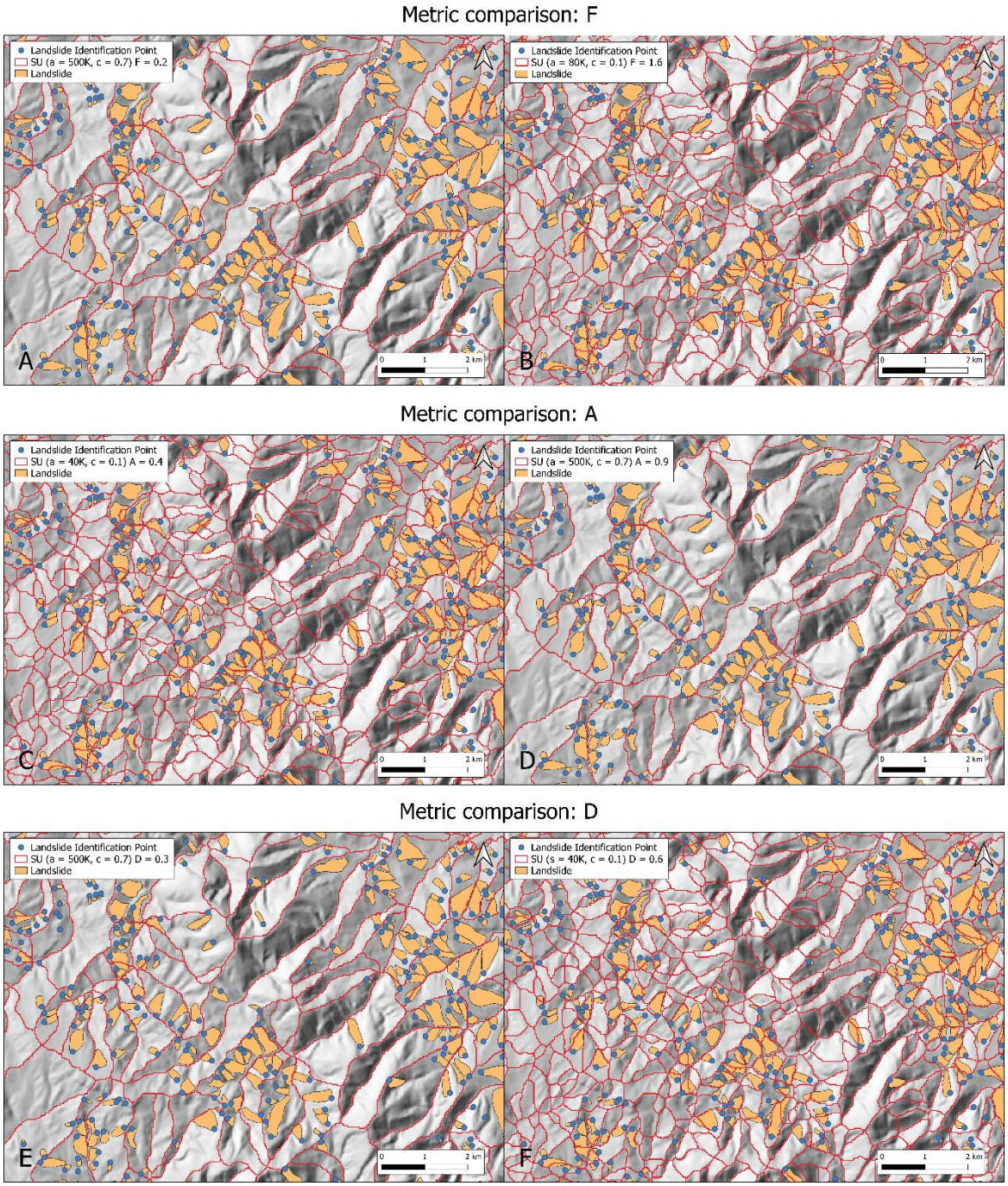


475

476 **Figure 11: Selection of SUs partition of a sub-portion of the study area AOIa. A) and B) The SUs partitions with the**
477 **lowest and the highest value of F respectively; C) and D) The SUs partitions with the lowest and the highest value of A**
478 **respectively; E) and F) The SUs partitions with the lowest and the highest value of D respectively.**

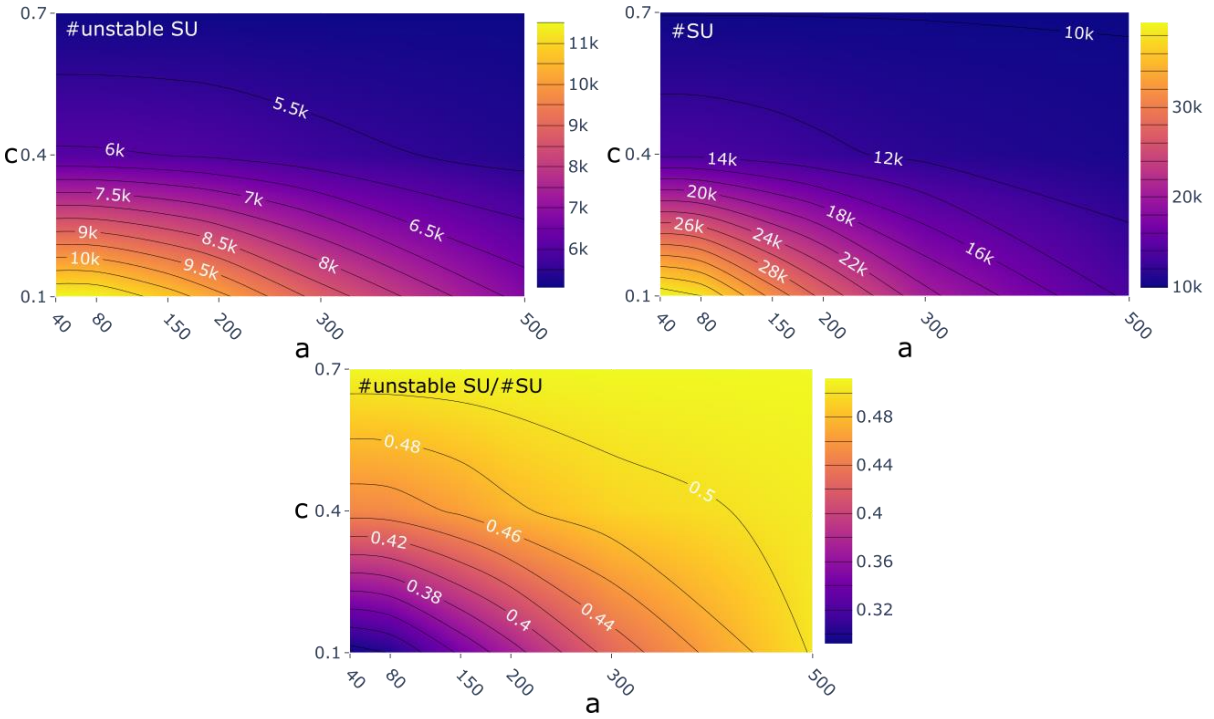


**Figure 12: Evolution of the portion of unstable SUs in the study area with varying values of *a* and *c*.**

All metrics unified in *S* maximizes their effect, as shown in an example in Figure 13 where the comparable differences explain the concept of the ration between the number and extension of landslides contained in the SUs. While it is difficult to minimize SU area as well as contain the landslide area, it is to be considered that the spatial and areal accuracy of landslide inventories can significantly affect the output since the best terrain partition is interpreted based on the dimensions and number of landslide polygons. In this case study, the PAI of Marche region has been used to test the methodology, and while the landslide inventory plays a crucial role, it has to be mentioned that the dataset used may come with limitations. The inventory has not been systematically updated for the mapped landslide areas and the dataset has been updated by reports from scientific literature, local authorities and projects of the municipalities (Costanzo and Irigaray, 2020). Nonetheless, the methodology remains compatible with landslide polygons and SUs supporting the selection of an optimal terrain partitioning.

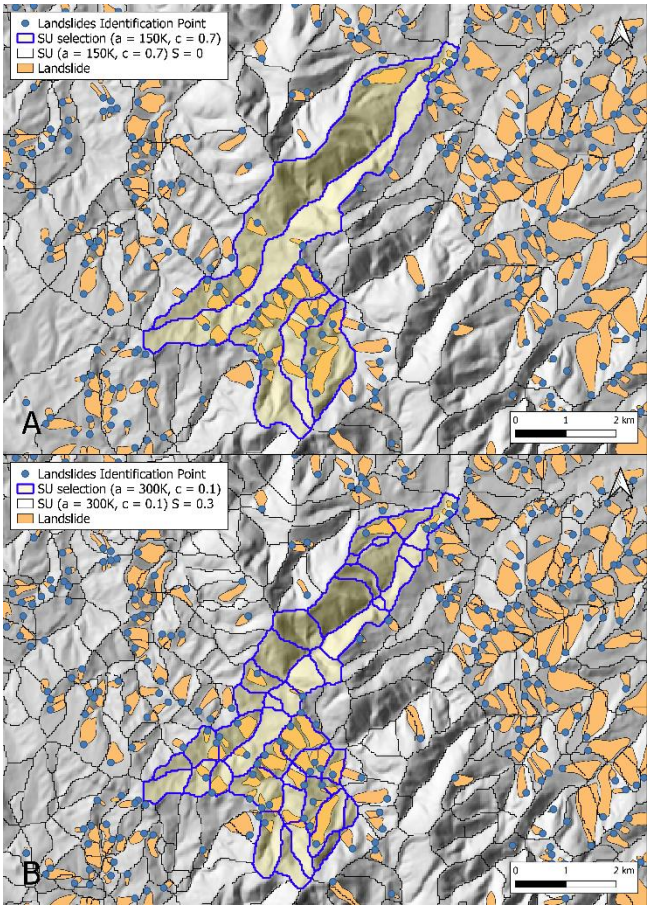


**Figure 13: SUs partitions of a sub-portion of the Marche study area (AOIa) compared to landslides distribution from the PAI. A) the SU partition (*a:* 150x10$^3$ m$^2$ and *c:* 0.7) with lowest value of *S*, B) the SU partition (*a:* 300 x10$^3$m$^2$ and *c*: 0.1) with highest value of *S*.**

Two susceptibility analyses have been carried out selecting the S-optimal and S-worst case SUs partitions. Since, the goal of this study is not to assess landslide susceptibility of the Marche region, but to investigate the potential effect of a thought-out SUs delineation for landslide susceptibility evaluated with largely used metrics such as AUC, F1-score and Cohen's Kappa score, the predisposing factors selected for the susceptibility analysis are not entirely representative of the geo-environmental conditions. In particular, not all predisposing factors (e.g., land use, vegetation indices and others) have been considered (see also Titti et al. 2024). Therefore, the cross-validation results (Figure 9A) of the susceptibility map (Figure 8A) calculated with the optimal SU subdivision are not performing high in the metrics considered (AUC = 0.68, F1 score = 0.6, K = 0.23 on average). Nevertheless, it is interesting to highlight the trend of the relation between the mapping unit extension and the AUC value along with other metrics.

AUC is calculated as the integral of the ROC curve. The ROC curve depends on the balance between unstable units and stable units in the training dataset, thus, the higher is the ratio between the number of unstable SUs and the total number of SUs, higher is the AUC because higher is the learning capacity of the model to recognize TP mapping units increasing the True Positive Rate (TPR) value of the ROC curve. In the 18 combinations selected, to investigate the highest-performing *a* and *c* values for SUs delineation, we haven't changed the landslide number but the extension of the SUs whose trend is visible through the number of SUs pattern in Figure 14. Considering all the combinations of *a* and *c* performed in our experiment, the higher the extension of the mapping units, the

higher the proportion between the number of unstable units and the number of all the mapping units and higher the AUC (Figure 14). Same considerations can be done for the F1 score, and the Cohen's Kappa index whose behaviors follow similar trend of the AUC.

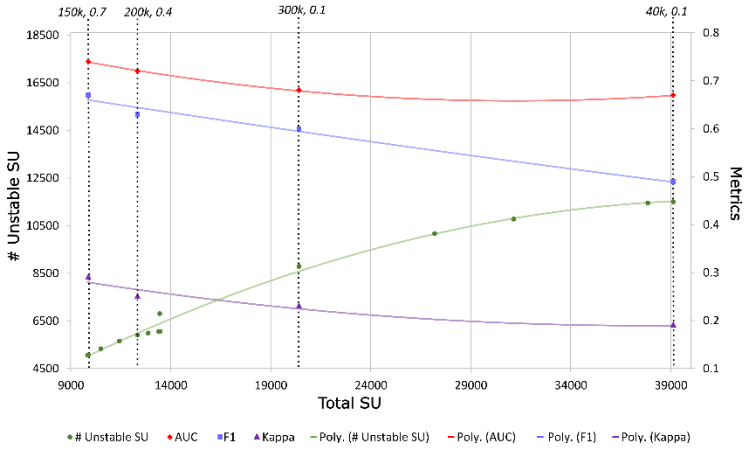


**Figure 14: Trend of the number of unstable and total SUs comparison (of 18 combinations for *a* and *c*) and the behavior of the metrics resulting from the landslide susceptibility analysis. The parameters (*a, c*) are labelled along the performance metrics to represent the respective trend.**

Therefore, at least in the experiments made for this study, the metrics selected are not suitable for comparing susceptibility maps directly because the training datasets are differently balanced. Nevertheless, a comparison between the S-optimal and S-worst case susceptibility maps, as shown in Figure 8A and Figure 8C respectively, can still be made. Graphically, the maps exhibit a similar spatial pattern of landslide probability of occurrence. This is further supported by the fact that the number of TN units relative to unstable units is nearly the same, at 13% and 12% for the S-optimal and the S-worst case, respectively. The primary distinction lies in the susceptibility value, which is on average lower in the S-optimal delineation than in the S-worst case. This difference is attributed to the overestimation of unstable units in the S-worst case due to the imbalance between stable and unstable units.

## 6. Conclusions

This study encompasses DEM utilization from the viewpoint of fine-scale morphology and terrain sub-division into mapping units in the frame of regional predictive landslide modelling. The aim is to compare freely available global and national DEMs from which morphological landslide predisposing factors and optimized terrain partition in slope units are derived to map landslide susceptibility. Therefore, the investigation initially identified the optimal DEM among the available ones and then selected the optimal SUs partition in the alternative combinations generated.

The global DEMs (ALOS, COP, FABDEM) and TINITALY resampled at 30m have shown considerable differences with respect to the reference DEM (an airborne LiDAR resampled at 30m pixel size) in the selected geomorphometric derivatives in AOIb. Concerning the SUs delineation, the TINITALY30m has shown the best performance thus, it has been selected to generate 18-parameter SUs subdivisions in AOIa. To define the optimal SUs delineation, a novel method has been proposed, which evaluates the SUs alternatives on the base of internal aspect homogeneity/external heterogeneity, landslides numerosity and landslides extension. According to the *S*

metric (Eq. 6), the SUs partition generated with $c$ equal to 0.1 and $a$ equal to $300x10^3$ $m^2$ results in the optimal subdivision, contrasting with $c$ equal to 0.7 and $a$ equal to $150x10^3$ $m^2$ as the worst case one.

Ultimately, to understand the effect of the terrain partition on the landslide susceptibility model, we have performed the S-optimal and the S-worst case landslide susceptibility. It is understood that the performance metrics (AUC, F1, K) of the landslide susceptibility models do not necessarily equate with the $S$ metric performance. Indeed, AUC, F1 and K depict opposite trends as compared with the $S$ metric.

Though only TINITALY30m has been used in extending the analysis for SU experiments, COP, as the second-best performing DEM for fine-scale morphology, can also be considered in future studies. A holistic comparison could help evaluate its effectiveness in landslide susceptibility studies. Moreover, since the result of the $S$-method depends on the landslide inventory, further research would pave the way for space-time inventories performing multi-temporal SUs delineations to reach the best terrain delineation for slope failure prediction. Developing space-time landslide inventories and adapting SUs delineation for dynamic, evolving terrains could significantly enhance the predictive capability of landslide models. Ultimately, continued innovation in DEM selection, SU partitioning methods, and landslide inventory development will contribute to more effective landslide risk management strategies and mitigation efforts.

## Data availability

The optimal SUs partition of the Marche study area (AOIa) is freely available at Ahmed and Titti (2024).

DEMs used: COP and ALOS (https://opentopography.org/), FABDEM (https://data.bris.ac.uk/data/dataset/25wfy0f9ukoge2gs7a5mqpq2j7), TINITALY (https://tinitaly.pi.ingv.it/Download_Area1_0.html).

## Author contributions

MA: Conceptualization, Methodology, Formal analysis, Writing - Original Draft; GT: Conceptualization, Methodology, Formal analysis, Writing - Original Draft, Funding acquisition; ST: Methodology, Formal analysis, Writing - Review & Editing; LB: Writing - Review & Editing, Supervision; MF: Writing - Review & Editing, Supervision.

## Competing interests

The authors declare that they have no conflict of interest.

## Acknowledgements

This study was carried out within the RETURN Extended Partnership and received funding from the European Union Next480 Generation EU (National Recovery and Resilience Plan – NRRP, Mission 4, Component 2, Investment 1.3 – D.D. 1243 2/8/2022, PE0000005).

571

## References


Abrams, M., Bailey, B., Tsu, H., and Hato, M.: The ASTER Global DEM, Photogramm Eng Remote Sensing, 76, 344–348, 2010.

Ahmed, M. and Titti, G.: Slope Units delineation for Marche region in Italy [Dataset], https://doi.org/https://doi.org/10.5281/zenodo.13769104, 2024.

Ahmed, M., Tanyas, H., Huser, R., Dahal, A., Titti, G., Borgatti, L., Francioni, M., and Lombardo, L.: Dynamic rainfall-induced landslide susceptibility: A step towards a unified forecasting system, International Journal of Applied Earth Observation and Geoinformation, 125, 103593, https://doi.org/10.1016/J.JAG.2023.103593, 2023.

Albertella, A., Barzaghi, R., Carrion, D., and Maggi, A.: The joint use of gravity data and GPS/levelling undulations in geoid estimation procedures, Bollettino di Geodesia e Scienze Affini, 67, 49–59, 2008.

Alvioli, M., Marchesini, I., Reichenbach, P., Rossi, M., Ardizzone, F., Fiorucci, F., and Guzzetti, F.: Automatic delineation of geomorphological slope units with r.slopeunits v1.0 and their optimization for landslide susceptibility modeling, Geosci Model Dev, 9, 3975–3991, https://doi.org/10.5194/gmd-9-3975-2016, 2016.

Barzaghi, R. and Carrion, D.: Testing EGM2008 in the Central Mediterranean area, in: External Quality Evaluation Reports of EGM08, International Association of Geodesy and International Gravity Field Service, 133–143, 2009.

Barzaghi, R., Borghi, A., Carrion, D., and Sona, G.: Refining the estimate of the Italian quasi-geoid, Bollettino di Geodesia e Scienze Affini, 50, 145–159, 2007.

Becek, K.: Assessing global digital elevation models using the runway method: The advanced spaceborne thermal emission and reflection radiometer versus the shuttle radar topography mission case, IEEE Transactions on Geoscience and Remote Sensing, 52, 4823–4831, https://doi.org/10.1109/TGRS.2013.2285187, 2014.

Bielski, C., Lopez-Vazquez, C., Grohmann, C. H., Guth, P. L., Hawker, L., Gesch, D., Trevisani, S., Herrera-Cruz, V., Riazanoff, S., Corseaux, A., Reuter, H. I., and Strobl, P.: Novel approach for ranking DEMs: Copernicus DEM improves one arc second open global topography, IEEE Transactions on Geoscience and Remote Sensing, 62, 1–22, https://doi.org/10.1109/TGRS.2024.3368015, 2024.

Van den Bout, B., Lombardo, L., Chiyang, M., van Westen, C., and Jetten, V.: Physically-based catchment-scale prediction of slope failure volume and geometry, Eng Geol, 284, 105942, https://doi.org/10.1016/J.ENGGEO.2020.105942, 2021.

Brenning, A.: Spatial prediction models for landslide hazards: review, comparison and evaluation, Natural Hazards and Earth System Sciences, 5, 853–862, https://doi.org/10.5194/NHESS-5-853-2005, 2005.

Brock, J., Schratz, P., Petschko, H., Muenchow, J., Micu, M., and Brenning, A.: The performance of landslide susceptibility models critically depends on the quality of digital elevation models, Geomatics, Natural Hazards and Risk, 11, 1075–1092, https://doi.org/10.1080/19475705.2020.1776403, 2020.

Caglar, B., Becek, K., Mekik, C., and Ozendi, M.: On the vertical accuracy of the ALOS world 3D-30m digital elevation model, Remote Sensing Letters, 9, 607–615, https://doi.org/10.1080/2150704X.2018.1453174, 2018.

Carrara, A., Cardinali, M., Detti, R., Guzzetti, F., Pasqui, V., and Reichenbach, P.: GIS techniques and statistical models in evaluating landslide hazard, Earth Surf Process Landf, 16, 427–445, https://doi.org/10.1002/ESP.3290160505, 1991.

Catani, F., Lagomarsino, D., Segoni, S., and Tofani, V.: Landslide susceptibility estimation by random forests technique: Sensitivity and scaling issues, Natural Hazards and Earth System Sciences, 13, 2815–2831, https://doi.org/10.5194/NHESS-13-2815-2013, 2013.

Chaplot, V., Darboux, F., Bourennane, H., Leguédois, S., Silvera, N., and Phachomphon, K.: Accuracy of interpolation techniques for the derivation of digital elevation models in relation to landform types and data density, Geomorphology, 77, 126–141, https://doi.org/10.1016/J.GEOMORPH.2005.12.010, 2006.

Chen, Z., Ye, F., Fu, W., Ke, Y., and Hong, H.: The influence of DEM spatial resolution on landslide susceptibility mapping in the Baxie River basin, NW China, Natural Hazards, 101, 853–877, https://doi.org/10.1007/S11069-020-03899-9/FIGURES/12, 2020.

Claessens, L., Heuvelink, G. B. M., Schoorl, J. M., and Veldkamp, A.: DEM resolution effects on shallow landslide hazard and soil redistribution modelling, Earth Surf Process Landf, 30, 461–477, https://doi.org/10.1002/ESP.1155, 2005.

Corti, M., Francioni, M., Abbate, A., Papini, M., and Longoni, L.: ANALYSIS AND MODELLING OF THE SEPTEMBER 2022 FLOODING EVENT IN THE MISA BASIN, Italian Journal of Engineering Geology and Environment, 69–76, https://doi.org/10.4408/IJEGE.2024-01.S-08, 2024.

Costanzo, D. and Irigaray, C.: Comparing Forward Conditional Analysis and Forward Logistic Regression Methods in a Landslide Susceptibility Assessment: A Case Study in Sicily, Hydrology, 7, 37, https://doi.org/10.3390/HYDROLOGY7030037, 2020.

Crema, S., Llena, M., Calsamiglia, A., Estrany, J., Marchi, L., Vericat, D., and Cavalli, M.: Can inpainting improve digital terrain analysis? Comparing techniques for void filling, surface reconstruction and geomorphometric analyses, Earth Surf Process Landf, 45, 736–755, https://doi.org/10.1002/ESP.4739, 2020.

Cruden, D. M. and Varnes, D. J.: Landslide Types and Processes, Transportation Research Board, U.S. National Academy of Sciences, Special Report, 36–75 pp., 1996.

Elia, L., Castellaro, S., Dahal, A., and Lombardo, L.: Assessing multi-hazard susceptibility to cryospheric hazards: Lesson learnt from an Alaskan example, Science of The Total Environment, 898, 165289, https://doi.org/10.1016/J.SCITOTENV.2023.165289, 2023.

European Space Agency: Copernicus Global Digital Elevation Model, https://doi.org/10.5069/G9028PQB, 2024.

Fawcett, T.: An introduction to ROC analysis, Pattern Recognit Lett, 27, 861–874, https://doi.org/10.1016/J.PATREC.2005.10.010, 2006.

Fenton, G. A., McLean, A., Nadim, F., and Griffiths, D. V.: Landslide hazard assessment using digital elevation models, Canadian Geotechnical Journal, 50, 620–631, https://doi.org/10.1139/CGJ-2011-0342, 2013.

Florinsky, I. V.: Accuracy of local topographic variables derived from digital elevation models, International Journal of Geographical Information Science, 12, 47–62, https://doi.org/10.1080/136588198242003, 1998.

Florinsky, I. V., Skrypitsyna, T. N., Trevisani, S., and Romaikin, S. V.: Statistical and visual quality assessment of nearly-global and continental digital elevation models of Trentino, Italy, Remote Sensing Letters, 10, 726–735, https://doi.org/10.1080/2150704X.2019.1602790, 2019.

Gesch, D. B.: Best practices for elevation-based assessments of sea-level rise and coastal flooding exposure, Front Earth Sci (Lausanne), 6, https://doi.org/10.3389/FEART.2018.00230/BIBTEX, 2018.

Gesch, D. B., Evans, G. A., Oimoen, M. J., and Arundel, S.: The National Elevation Dataset, in: Digital Elevation MoFDigital Elevation Model Technologies and Applications: The DEM Users Manual, American Society for Photogrammetry and Remote Sensing, 83–110, 2018.

Grohmann, C. H.: Evaluation of TanDEM-X DEMs on selected Brazilian sites: Comparison with SRTM, ASTER GDEM and ALOS AW3D30, Remote Sens Environ, 212, 121–133, https://doi.org/10.1016/J.RSE.2018.04.043, 2018.

Grohmann, C. H., Smith, M. J., and Riccomini, C.: Multiscale analysis of topographic surface roughness in the Midland Valley, Scotland, IEEE Transactions on Geoscience and Remote Sensing, 49, 1200–1213, https://doi.org/10.1109/TGRS.2010.2053546, 2011.

Guisan, A., Weiss, S. B., and Weiss, A. D.: GLM versus CCA spatial modeling of plant species distribution, Plant Ecol, 143, 107–122, https://doi.org/10.1023/A:1009841519580/METRICS, 1999.

Guth, P. L. and Geoffroy, T. M.: LiDAR point cloud and ICESat-2 evaluation of 1 second global digital elevation models: Copernicus wins, Transactions in GIS, 25, 2245–2261, https://doi.org/10.1111/TGIS.12825, 2021.

Guth, P. L., Trevisani, S., Grohmann, C. H., Lindsay, J., Gesch, D., Hawker, L., and Bielski, C.: Ranking of 10 Global One-Arc-Second DEMs Reveals Limitations in Terrain Morphology Representation, Remote Sens (Basel), 16, 3273, https://doi.org/10.3390/RS16173273, 2024.

Hawker, L., Neal, J., and Bates, P.: Accuracy assessment of the TanDEM-X 90 Digital Elevation Model for selected floodplain sites, Remote Sens Environ, 232, 111319, https://doi.org/10.1016/J.RSE.2019.111319, 2019.

Hawker, L., Uhe, P., Paulo, L., Sosa, J., Savage, J., Sampson, C., and Neal, J.: A 30 m global map of elevation with forests and buildings removed, Environmental Research Letters, 17, https://doi.org/10.1088/1748-9326/AC4D4F, 2022.

Hiller, J. K. and Smith, M.: Residual relief separation: digital elevation model enhancement for geomorphological mapping, Earth Surf Process Landf, 33, 2266–2276, https://doi.org/10.1002/ESP.1659, 2008.

Huang, F., Teng, Z., Guo, Z., Catani, F., and Huang, J.: Uncertainties of landslide susceptibility prediction: Influences of different spatial resolutions, machine learning models and proportions of training and testing dataset, Rock Mechanics Bulletin, 2, https://doi.org/10.1016/J.ROCKMB.2023.100028, 2023.

Isaaks, E. H. and Srivastava, R. Mohan.: Applied geostatistics, Oxford University Press, London, 1989.

Jaccard, P.: Etude comparative de la distribution florale dans une portion des Alpes et du Jura, 142nd ed., edited by: Bulletin de la Société vaudoise des sciences naturelles, Impr. Corbaz, 1901.

ALOS World 3D - 30m. V3.2: Distributed by OpenTopography. https://doi.org/10.5069/G94M92HB. Accessed: 2024-04-16, last access: 18 March 2024.

Jarvis, A., Guevara, E., Reuter, H. I., and Nelson, A. D.: Hole-filled SRTM for the globe : version 4, https://doi.org/10.2/JQUERY.MIN.JS, 2008.

Kakavas, M., Kyriou, A., and Nikolakopoulos, K. G.: Assessment of freely available DSMs for landslide-rockfall studies, in: Proceedings of SPIE, https://doi.org/10.1117/12.2573604, 2020.

Kamiński, M.: The Impact of Quality of Digital Elevation Models on the Result of Landslide Susceptibility Modeling Using the Method of Weights of Evidence, Geosciences (Basel), 10, https://doi.org/10.3390/GEOSCIENCES10120488, 2020.

Karakas, G., Kocaman, S., and Gokceoglu, C.: On the effect of dem quality for landslide susceptibility mapping, ISPRS Annals of the Photogrammetry, Remote Sensing and Spatial Information Sciences, V-3–2022, 525–531, https://doi.org/10.5194/ISPRS-ANNALS-V-3-2022-525-2022, 2022.

Kraemer, H. C.: Kappa Coefficient, Wiley StatsRef: Statistics Reference Online, 1–4, https://doi.org/10.1002/9781118445112.STAT00365.PUB2, 2015.

Liu, K., Song, C., Ke, L., Jiang, L., Pan, Y., and Ma, R.: Global open-access DEM performances in Earth's most rugged region High Mountain Asia: A multi-level assessment, Geomorphology, 338, 16–26, https://doi.org/10.1016/J.GEOMORPH.2019.04.012, 2019.

Loche, M., Alvioli, M., Marchesini, I., and Lombardo, L.: Landslide Susceptibility within the binomial Generalized Additive Model, in: European Geosciences Union (EGU23), https://doi.org/10.13140/RG.2.2.14089.62565, 2023.

Lombardo, L. and Tanyas, H.: Chrono-validation of near-real-time landslide susceptibility models via plug-in statistical simulations, Eng Geol, 278, https://doi.org/10.1016/J.ENGGEO.2020.105818, 2020.

Lombardo, L., Bakka, H., Tanyas, H., van Westen, C., Mai, P. M., and Huser, R.: Geostatistical Modeling to Capture Seismic-Shaking Patterns From Earthquake-Induced Landslides, J Geophys Res Earth Surf, 124, 1958–1980, https://doi.org/10.1029/2019JF005056, 2019.

Lombardo, L., Opitz, T., Ardizzone, F., Guzzetti, F., and Huser, R.: Space-time landslide predictive modelling, https://doi.org/10.1016/j.earscirev.2020.103318, October 2020.

Mahalingam, R. and Olsen, M. J.: Evaluation of the influence of source and spatial resolution of DEMs on derivative products used in landslide mapping, Geomatics, Natural Hazards and Risk, 7, 1835–1855, https://doi.org/10.1080/19475705.2015.1115431, 2016.

Meadows, M., Jones, S., and Reinke, K.: Vertical accuracy assessment of freely available global DEMs (FABDEM, Copernicus DEM, NASADEM, AW3D30 and SRTM) in flood-prone environments, Int J Digit Earth, 17, https://doi.org/10.1080/17538947.2024.2308734, 2024.

Muralikrishnan, S., Pillai, A., Narender, B., Reddy, S., Venkataraman, V. R., and Dadhwal, V. K.: Validation of Indian National DEM from Cartosat-1 Data, Journal of the Indian Society of Remote Sensing, 41, 1–13, https://doi.org/10.1007/S12524-012-0212-9/FIGURES/13, 2013.

Osama, N., Shao, Z., and Freeshah, M.: The FABDEM Outperforms the Global DEMs in Representing Bare Terrain Heights, Photogramm Eng Remote Sensing, 89, 613–624, https://doi.org/10.14358/PERS.23-00026R2, 2023.

Pawluszek, K. and Borkowski, A.: Impact of DEM-derived factors and analytical hierarchy process on landslide susceptibility mapping in the region of Rożnów Lake, Poland, Natural Hazards, 86, 919–952, https://doi.org/10.1007/S11069-016-2725-Y/FIGURES/26, 2017.

Pirasteh, S. and Li, J.: Landslides investigations from geoinformatics perspective: quality, challenges, and recommendations, Geomatics, Natural Hazards and Risk, 8, 448–465, https://doi.org/10.1080/19475705.2016.1238850, 2017.

Polidori, L. and Hage, M. El: Digital Elevation Model Quality Assessment Methods: A Critical Review, Remote Sens (Basel), 12, https://doi.org/10.3390/RS12213522, 2020.

Pulighe, G. and Fava, F.: DEM extraction from archive aerial photos: accuracy assessment in areas of complex topography, Eur J Remote Sens, 46, 363–378, https://doi.org/10.5721/EuJRS20134621, 2013.

Purinton, B. and Bookhagen, B.: Validation of digital elevation models (DEMs) and comparison of geomorphic metrics on the southern Central Andean Plateau, Earth Surface Dynamics, 5, 211–237, https://doi.org/10.5194/ESURF-5-211-2017, 2017.

Qin, C. Z., Bao, L. L., Zhu, A. X., Wang, R. X., and Hu, X. M.: Uncertainty due to DEM error in landslide susceptibility mapping, International Journal of Geographical Information Science, 27, 1364–1380, https://doi.org/10.1080/13658816.2013.770515, 2013.

Qiu, H., Zhu, Y., Zhou, W., Sun, H., He, J., and Liu, Z.: Influence of DEM resolution on landslide simulation performance based on the Scoops3D model, Geomatics, Natural Hazards and Risk, 13, 1663–1681, https://doi.org/10.1080/19475705.2022.2097451, 2022.

Reichenbach, P., Rossi, M., Malamud, B. D., Mihir, M., and Guzzetti, F.: A review of statistically-based landslide susceptibility models, Earth Sci Rev, 180, 60–91, https://doi.org/10.1016/J.EARSCIREV.2018.03.001, 2018.

Riley, S. J., Degloria, S. D., and Elliot, S. D.: A Terrain Ruggedness Index that Quantifies Topographic Heterogeneity, Intermountain Journal of Sciences, 5, 23–27, 1999.

Saleem, N., Enamul Huq, M., Twumasi, N. Y. D., Javed, A., and Sajjad, A.: Parameters Derived from and/or Used with Digital Elevation Models (DEMs) for Landslide Susceptibility Mapping and Landslide Risk Assessment: A Review, ISPRS Int J Geoinf, 8, 545, https://doi.org/10.3390/IJGI8120545, 2019.

Schlögel, R., Marchesini, I., Alvioli, M., Reichenbach, P., Rossi, M., and Malet, J. P.: Optimizing landslide susceptibility zonation: Effects of DEM spatial resolution and slope unit delineation on logistic regression models, Geomorphology, 301, 10–20, https://doi.org/10.1016/J.GEOMORPH.2017.10.018, 2018.

Singhal, A.: Modern Information Retrieval: A Brief Overview, IEEE Data Eng. Bull., 24, 35–43, 2001.

Steger, S., Moreno, M., Crespi, A., Zellner, P. J., Gariano, S. L., Brunetti, M. T., Melillo, M., Peruccacci, S., Marra, F., Kohrs, R., Goetz, J., Mair, V., and Pittore, M.: Deciphering seasonal effects of triggering and preparatory precipitation for improved shallow landslide prediction using generalized additive mixed models, Natural Hazards and Earth System Sciences, 23, 1483–1506, https://doi.org/10.5194/NHESS-23-1483-2023, 2023.

Strobl, P. A., Bielski, C., Guth, P. L., Grohmann, C. H., Muller, J. P., López-Vázquez, C., Gesch, D. B., Amatulli, G., Riazanoff, S., and Carabajal, C.: The digital elevation model intercomparison experiment demix, a community-based approach at global dem benchmarking, International Archives of the Photogrammetry, Remote Sensing and Spatial Information Sciences - ISPRS Archives, 395–400, https://doi.org/10.5194/ISPRS-ARCHIVES-XLIII-B4-2021-395-2021, 2021.

Takaku, J., Tadono, T., and Tsutsui, K.: Generation of high resolution global DSM from ALOS PRISM, International Archives of the Photogrammetry, Remote Sensing and Spatial Information

Sciences - ISPRS Archives, 40, 243–248, https://doi.org/10.5194/isprsarchives-XL-4-243-2014, 2014.

Tarquini, S., Isola, I., Favalli, M., Mazzarini, F., Bisson, M., Pareschi, M. T., and Boschi, E.: TINITALY/01: a new Triangular Irregular Network of Italy, Annals of Geophysics, 50, 407–425, https://doi.org/10.4401/ag-4424, 2007.

Tarquini, S., Isola, I., Favalli, M., Battistini, A., and Dotta, G.: TINITALY, a digital elevation model of Italy with a 10 meters cell size (Version 1.1) [Data set], https://doi.org/https://doi.org/10.13127/tinitaly/1.1, 2023.

Titti, G., Borgatti, L., Zou, Q., Cui, P., and Pasuto, A.: Landslide susceptibility in the Belt and Road Countries: continental step of a multi-scale approach, Environ Earth Sci, 80, 1–18, https://doi.org/10.1007/S12665-021-09910-1/FIGURES/11, 2021a.

Titti, G., van Westen, C., Borgatti, L., Pasuto, A., and Lombardo, L.: When Enough Is Really Enough? On the Minimum Number of Landslides to Build Reliable Susceptibility Models, Geosciences (Basel), 11, 469, https://doi.org/10.3390/GEOSCIENCES11110469, 2021b.

Titti, G., Sarretta, A., Lombardo, L., Crema, S., Pasuto, A., and Borgatti, L.: Mapping Susceptibility With Open-Source Tools: A New Plugin for QGIS, Front Earth Sci (Lausanne), 10, 842425, https://doi.org/10.3389/FEART.2022.842425/BIBTEX, 2022.

Trevisani, S. and Cavalli, M.: Topography-based flow-directional roughness: Potential and challenges, Earth Surface Dynamics, 4, 343–358, https://doi.org/10.5194/ESURF-4-343-2016, 2016.

Trevisani, S. and Rocca, M.: MAD: robust image texture analysis for applications in high resolution geomorphometry, Comput Geosci, 81, 78–92, https://doi.org/10.1016/J.CAGEO.2015.04.003, 2015.

Trevisani, S., Teza, G., and Guth, P.: A simplified geostatistical approach for characterizing key aspects of short-range roughness, Catena (Amst), 223, 106927, https://doi.org/10.1016/J.CATENA.2023.106927, 2023a.

Trevisani, S., Skrypitsyna, T. N., and Florinsky, I. V.: Global digital elevation models for terrain morphology analysis in mountain environments: insights on Copernicus GLO-30 and ALOS AW3D30 for a large Alpine area, Environ Earth Sci, 82, https://doi.org/10.1007/s12665-023-10882-7, 2023b.

Trevisani, S., Teza, G., and Guth, P. L.: Hacking the topographic ruggedness index, Geomorphology, 439, 108838, https://doi.org/10.1016/J.GEOMORPH.2023.108838, 2023c.

Van Westen, C. J., Rengers, N., Terlien, M. T. J., and Soeters, R.: Prediction of the occurrence of slope instability phenomena through GIS-based hazard zonation, Geologische Rundschau, 86, 404–414, https://doi.org/10.1007/S005310050149/METRICS, 1997.

Wilson, J. P. and Gallant, J. C. (Eds.): Terrain analysis : principles and applications, John Wiley & Sons, Inc, 2000.

Zhang, K., Gann, D., Ross, M., Robertson, Q., Sarmiento, J., Santana, S., Rhome, J., and Fritz, C.: Accuracy assessment of ASTER, SRTM, ALOS, and TDX DEMs for Hispaniola and implications for mapping vulnerability to coastal flooding, Remote Sens Environ, 225, 290–306, https://doi.org/10.1016/J.RSE.2019.02.028, 2019.

Zingaro, M., La Salandra, M., Colacicco, R., Roseto, R., Petio, P., and Capolongo, D.: Suitability assessment of global, continental and national digital elevation models for

geomorphological analyses in Italy, Transactions in GIS, 25, 2283–2308, https://doi.org/10.1111/TGIS.12845, 2021.